SMHI

Meteorologi

Nr 128, 2007

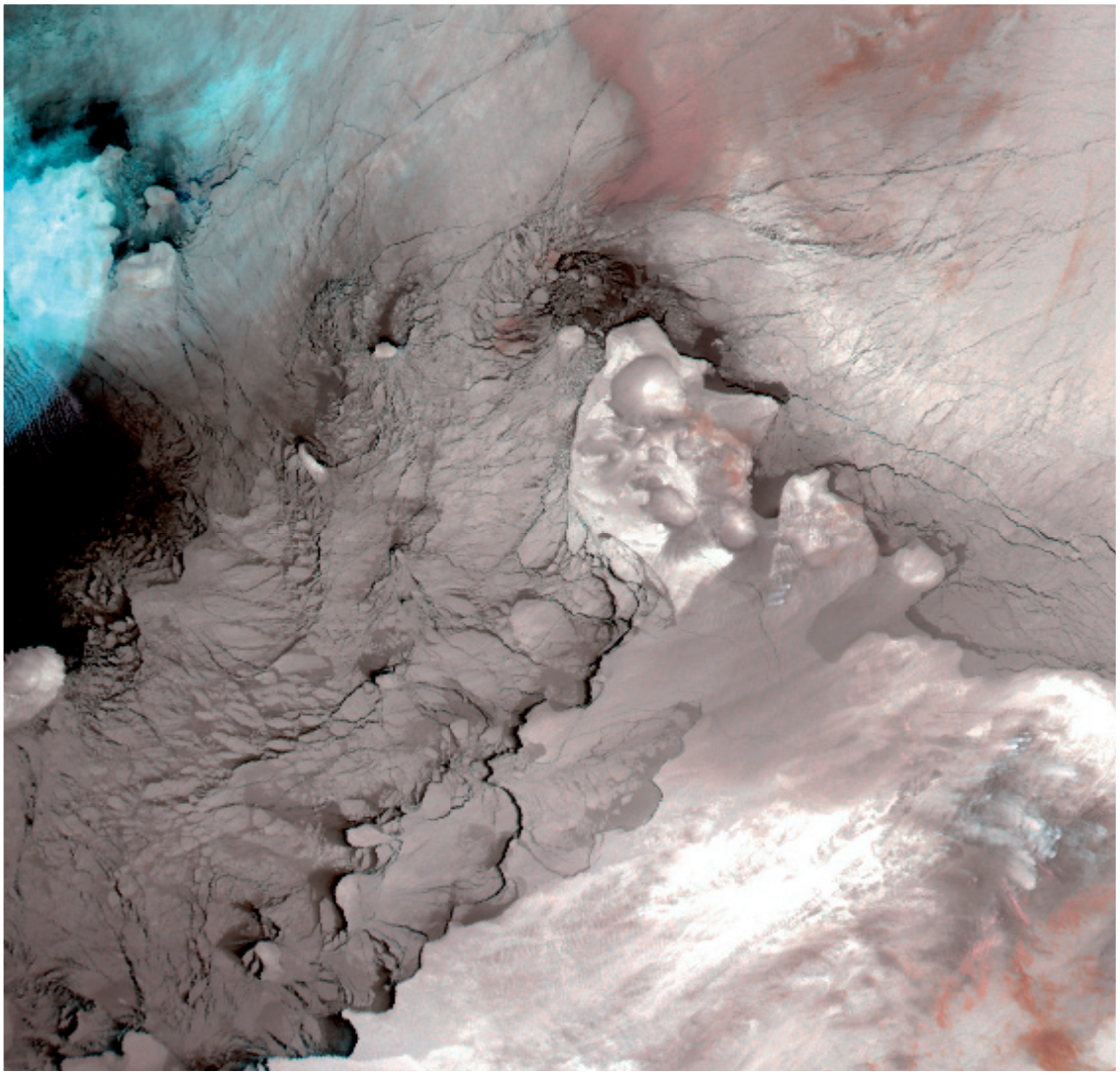

Prototyping an improved PPS cloud detection for the Arctic polar night

Salomon Eliasson, Anke Tetzlaff and Karl-Göran Karlsson

Meteorologi
Nr 128, 2007

Prototyping an improved PPS cloud detection for the Arctic polar night

Salomon Eliasson, Anke Tetzlaff and Karl-Göran Karlsson

Cover: A typical infrared RGB composite image (AVHRR channels at 3.7 µm, 11 µm and 12 µm) over the inner Arctic region during the polar night. The image from the NOAA-18 satellite shows typical polar night conditions close to the Russian island Severnaya Zemlya (covering the area denoted ibla_79n90e in Figure 2) on 31st of January 2007 at 03:09 UTC. Notice that the image is predominantly cloud free. However, there are patterns in the image that even the human eye (normally superior to any automatic image interpretation scheme) has difficulties to separate from typical cloud features. The only obvious signs of clouds are some thin high clouds in the upper right corner (bluish appearance) and also some thin low clouds in the upper right part and in the lower right corner (reddish appearance). How will an automatic multispectral cloud detection method treat such a situation? Find out later in Section 6!

Report Summary / Rapportsammanfattning

Issuing Agency/Utgivare	Report number/Publikation
SMHI S-601 76 NORRKÖPING Sweden	Meteorologi nr 128
	Report date/Utgivningsdatum September 2007

Author (s)/Författare

Salomon Eliasson, Anke Tetzlaff and Karl-Göran Karlsson

Title (and Subtitle/Titel

Prototyping an improved PPS cloud detection for the Arctic polar night

Abstract/Sammandrag

A new Polar Platform Systems (PPS) Cloud Mask (CM) test sequence is required for improving cloud detection during Arctic winter conditions. This study introduces a test sequence, called Ice Night Sea (INS), that to a greater extent successfully detects clouds over ice surfaces and which is less sensitive to cloud free misclassification.

The test sequence uses a combination of Numerical Weather Prediction (NWP) fields and Advanced Very High Resolution Radiometer (AVHRR) satellite data. Only the infrared (IR) AVHRR channels can be exploited during night conditions. Training target data from winter 2001-2002, collected over a large area north of the Atmospheric Radiation Measurement (ARM) site at Barrow, Alaska, were used to assess the general atmospheric state of the Arctic and to perform a qualitative validation of CM test sequences. Results clearly show that the atmospheric conditions during Arctic winter severely hamper cloud detection efforts. Very cold surface temperatures and immense surface temperature inversions lead to a diminished separability between surfaces and clouds. One particular problem is that the IR brightness temperatures for the shortest wavelength (3.7μm - henceforth T37) are strongly affected by noise. The use of an IR noise filter was shown to improve results significantly. In addition, the problem of misclassifying cracks in the pack ice as Cirrus clouds was basically solved by using a dedicated filter using the local variance of T37.

Using an inverse version of a typical daytime Cirrus test (based on just two IR channels and normally applied successfully outside the Arctic region), it is shown that we can detect a substantial part of the warm semi-transparent clouds commonly found in the Arctic.

Running the test sequences on training target data revealed an improvement in correct cloud free target classification of around 30% but only a marginal improvement for cloudy training targets. However, visual inspection of results obtained for about 50 scenes covering a large part of the Arctic region in January 2007 clearly indicated improvements also for the cloudy portion of the scenes. The INS CM test sequence awaits a more rigorous and quantitative validation, e.g. based on comparisons with CLOUDSAT/CALIPSO satellite data sets.

Key words/sök-, nyckelord

NWCSAF, PPS, AVHRR cloud detection, Arctic

Supplementary notes/Tillägg	Number of pages/Antal sidor	Language/Språk
	37	Engelska

ISSN and title/ISSN och titel

0283-7730 SMHI Meteorologi

Report available from/Rapporten kan köpas från:

SMHI
S-601 76 NORRKÖPING
Sweden

1 INTRODUCTION AND BACKGROUND 1

2 INTRODUCTION TO THE PPS CLOUD MASK ALGORITHM – NIGHT CONDITIONS OVER OCEAN 2

2.1 IMAGE FEATURE DEFINITIONS 2
2.2 THE CURRENT PPS NIGHT SCHEME OVER ICE-FREE OCEAN 3

3 STUDIES OF ARCTIC TRAINING TARGETS 5

3.1 SELECTION OF TARGETS 5
3.2 OVERALL SURFACE TEMPERATURE CONDITIONS FOR THE STUDIED PERIOD 5
3.3 SPECIFIC STUDIES OF THE PERFORMANCE OF THE T11TS FEATURE 7
3.4 SPECIFIC STUDIES OF THE PERFORMANCE OF THE T37T11 FEATURE 9
3.5 SPECIFIC STUDIES OF THE PERFORMANCE OF THE T11T12 FEATURE 10
3.6 SPECIFIC STUDIES OF THE PERFORMANCE OF TEXTURE FEATURES 16

4 PPS NIGHT SEA (NS) CM RESULTS ON TRAINING TARGETS 18

5 CREATION OF A NEW ICE NIGHT SEA (INS) TEST SEQUENCE 19

5.1 BASIC IDEAS FOR A MODIFIED CLOUD MASK METHOD 19
5.2 THE FINALLY PROPOSED INS CM TEST SEQUENCE 20
5.3 THE USE OF LOCAL TEXTURE FEATURES 21
5.4 DETAILED EXPLANATION OF TESTS IN THE INS CM TEST SEQUENCE 26

6 DEMONSTRATION AND VALIDATION OF INS CM RESULTS 27

7 DISCUSSION AND FUTURE PLANS 36

REFERENCES 37

1 Introduction and background

One of the tasks of the EUMETSAT Climate Monitoring SAF project (CM-SAF, see www.cmsaf.dwd.de and Schulz et al., 2005) is to provide monthly cloud climatologies from meteorological satellite data. Cloud information is derived from multispectral analysis of imagery from the NOAA AVHRR (Advanced Very High Resolution Radiometer) and METEOSAT SEVIRI (Spinning Enhanced Visible and InfraRed Imager) sensors. Corresponding cloud products from NOAA AVHRR data have been produced over the Initial Baseline Area (Figure 1) since January 2005 while production of similar products from SEVIRI started in September 2005. SEVIRI products over the full METEOSAT field of view (SEVIRI full disk – denoted MSG Area in Figure 1) is introduced in summer 2007.

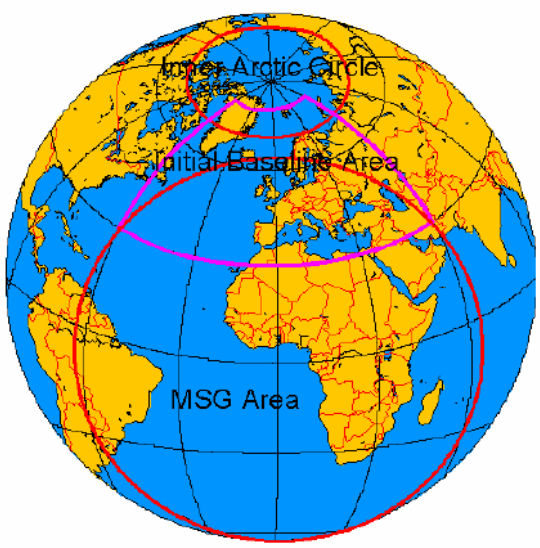

Figure 1. *Processing areas of the Climate Monitoring SAF.*

The mission at hand in this study has been to prepare for operational CM-SAF production of cloud products in the Arctic region (denoted Inner Arctic Circle in Figure 1). The current plan is to start with operational production in 2008 or 2009. Specifically, this particular study focuses on improvements of the cloud processing scheme under polar night conditions, i.e., for conditions were only infrared radiance measurements from satellite sensors are available and when the studied region is dominated by very cold snow and ice surfaces. Such conditions are known to be particularly difficult to cope with for traditional multispectral cloud processing schemes, mainly because of the fact that the Earth's surface is predominantly colder than the present clouds. An additional and complicating circumstance is that Arctic clouds are often composed of a mixture of supercooled water droplets and ice crystals. A third complicating factor is the frequent presence of isolated ice particles ("diamond dust") in near-surface atmospheric layers.

Cloud detection, cloud type labelling and cloud (top) height determination using polar NOAA AVHRR data is accomplished in the CM-SAF by use of the Polar Platform System (PPS) cloud processing software in the CM-SAF. This software was developed in the Nowcasting SAF project (NWC-SAF- see http://nwcsaf.inm.es) and details of the algorithm and its initial validation are given by Dybbroe et al., (2004a and 2004b). Operational processing in the CM-

SAF has been based on PPS version 1.0 for the period January 2005 to December 2006. The processing system was upgraded to PPS version 1.1 in January 2007. The current study has been based upon results from the next release of PPS; version 2.0. Further modifications aim at an upgraded PPS version (i.e. version 2.1) which would include adaptations for the Inner Arctic. The plan is to officially release this version to external users in January 2008.

This report will deal almost exclusively with polar night results of the PPS cloud mask (hereafter denoted CM) over the ice covered ocean. The basic idea is that in the finally upgraded PPS scheme we will utilise additional ancillary information (from external sources) on sea ice occurrence and then only apply the envisaged PPS modifications for ice covered regions.

Only the performance of the basic cloud detection will be discussed here. Studies of the other cloud products have been initiated but will be reported later. However, since the CM results are used as a major input data source to the other PPS cloud products we believe that improvements of the CM product will be significantly reflected in the quality of Cloud Type and Cloud Top products. It should also be mentioned that a similar PPS study has previously been made regarding available AVHRR data and PPS processing for polar day conditions (Sus, 2007).

In Section 2, we first give a very short introduction to the current PPS cloud detection scheme over ocean surfaces at night and its most important tests applied to image data. In relation to this, the commonly used image features are also described. Section 3 describes then extensive studies of Arctic conditions by the definition and analysis of special training targets in AVHRR imagery. It includes also some studies of some of the associated ancillary data sets over the studied region used by PPS for cloud processing. Following in Section 4 are the results of how the current available PPS scheme behaves when being faced with the Arctic polar night conditions. In Section 5 the proposed modifications to the PPS scheme for achieving improved results are introduced. Section 6 demonstrates results with such a modified PPS software for a number of case studies and for a monthly test dataset from January 2007. Finally, Section 7 discussed the main results and outlines the future implementation and validation of the modified PPS scheme.

2 Introduction to the PPS cloud mask algorithm – night conditions over ocean

We have here used the most recent official release of the PPS software package (NWC-SAF PPS version 2.0). Before describing in detail the basic night-time cloud detection algorithm applied over ocean surfaces we need to introduce some definitions regarding the used image features and the associated ancillary datasets.

2.1 Image feature definitions

Concerning the measured radiances of the three available infrared channels of the AVHRR instrument, we will consistently use them as being defined by their equivalent brightness temperatures (using the Planck function). Consequently, for the infrared AVHRR channels at 3.7 μm, 11 μm and 12 μm we will use their radiances defined as corresponding brightness temperatures denoted **T37**, **T11** and **T12**. Furthermore, if defining image features as a brightness temperature difference we will denote this difference as **TXXTYY** where **XX** and **YY** denotes original spectral channels. For example, **T37T12** denotes the brightness temperature difference between AVHRR channels at 3.7 μm and 12 μm.

The **T11** brightness temperature will also be compared to ancillary data from the ECMWF model. Thus, we use the notation **T11TS** to denote the temperature difference between **T11** and the ECMWF-analysed surface temperature. The latter is defined as the *skin temperature* (ECMWF GRIB parameter 235) in order to take into account that the satellite-measured radiance from an Earth surface is emitted according to the temperature of the uppermost thin layer of the ground or ocean.

Some attempts are also made to account for the local-scale brightness temperature variability in the images. Normally, a high variability over an otherwise ice-free ocean indicates presence of fractional clouds. Tests to detect such clouds are normally called *homogeneity tests*. The PPS use of homogeneity tests is accomplished by defining a new feature image created by calculating the brightness temperature variance within a 5x5 pixel window. This texture feature is normally denoted by adding the suffix **_text**. For example, the corresponding texture feature for **T11** (brightness temperature at 11 μm) is **T11_text**. Similar homogeneity test can also be applied to brightness temperature images (e.g. **T37T12_text**).

2.2 The current PPS night scheme over ice-free ocean

The Night Sea (NS) CM scheme yields CM value = 1 for cloud-free conditions, CM value = 2 if the pixel is deemed to be cloud contaminated or filled with semi-transparent clouds and CM = 3 if the pixel is deemed to be filled with opaque clouds. Notice that the intended use of NS CM is over ice free ocean (assuming a dark and relatively warm background for clouds) and it is therefore very likely that it will fail under ice-covered conditions.

In short, the current test sequence of the NS CM (version 1.6 of the Cloud Mask algorithm as included in PPS version 2.0) is as follows (**K** = Kelvin):

NS CM test sequence (V1.6):

1) watercloudTest (CM = 2) if **T11T37 > 0.3K**

*(Water clouds are colder in **T37** due to the fact that they are poorer black body radiators than at **T11** due to their ability during daytime to reflect solar radiation at wavelength 3.7 μm)*

2) thinCirrusPrimaryTest (CM = 2) if **T37T12 > 2.3K**

*(Semi-transparent Cirrus clouds are normally colder in **T12** than in **T37** due to a higher transmissivity at wavelength 3.7 μm)*

3) textureNightTest (CM = 2**)** if **T11_text > 0.8K & T37T12_text > 0.9K**

(Spatial homogeneity test, i.e. it will detect fractional clouds over open sea due to the induced high local variance of brightness temperatures and brightness temperature differences)

4) coldCloudTest (CM = 3) if **T11TS < -16 K & TS > 274K**

*(This test is aimed at detecting clouds that are significantly colder than the surface but notice that it will not work over ice due the restriction of **TS**)*

5) coldWatercloudTest (CM = 3**)** if **T11T37 > 0.3K & T11TS < -8K**

(This test is a special case of test 1 above having an additional requirement that these clouds must be more than 8 K colder than the surface – often the case for clouds of type Stratocumulus or Altocumulus. The main difference compared to test 1 is that if we simultaneously measure T11TS differences larger than 8K we are more confident that this is a thick cloud with a cold cloud top. Thus, we then change the labelling from CM=2 to CM=3).)

6) (extra) coldCloudTest (CM = 3**)** if **T11Ts < -8K & TS > 274K**

*(This test is a special case of test 4 above with lower restrictions on temperature difference compared to **TS**. The idea to split tests 4 and 6 like this is to still allow for thick water clouds being properly identified using the test 5.)*

7) "Clear sky terminator" (CM = 2**)** if **T11 < 270K**

(The name of this test is a clear indication that the NS test sequence is not designed for conditions with ice covered ocean. All remaining ice areas will here be interpreted as being cloud contaminated! It was introduced to ensure that when using the PPS CM product as a pre-processor in Sea Surface Temperature retrieval applications (e.g. as in the Ocean and Sea Ice SAF – OSISAF – see www.osi-saf.org) the CM should only identify ice-free and cloud-free ocean surfaces.)

Notice that the names of the tests indicate the primary purpose of the cloud test. Also, notice that tests are given in the exact chronological order of how they are applied to measurements. The general idea is that if a test is positive (and within safe margins) the testing is stopped and the indicated CM-value is returned. For tests that are positive but close to threshold values, the suggested CM-value is assigned with a low quality warning and the testing is continued to see if some of the remaining tests are more confidently positive.

Of importance in the interpretation of the listed tests above is that the static threshold offsets (given at the right-hand side of inequality symbols) for the difference features **T11T37** and **T37T12** have to be applied only **after** also having added so-called *dynamical thresholds*. The dynamical thresholds are the corresponding differences that have to be expected under cloud-free conditions because of atmospheric effects (e.g. absorption in water vapour in the atmosphere). These are pre-calculated and defined in Look-up tables for PPS (see description by Dybbroe et al., 2004a). The threshold values listed above is often referred to as *static threshold offsets*. By using this terminology we can define the finally applied thresholds as

Final thresholds = dynamical thresholds + static threshold offsets

The static threshold offsets are used as tuning parameters of PPS. For some tests (like **T11TS**) they contain a safety margin caused by the current uncertainty in the NWP-analysed surface temperature parameter **TS**.

3 Studies of Arctic training targets

3.1 Selection of targets

For studying more in detail how the chosen PPS-analysed image features (introduced in the previous section) and the associated ancillary information behaves in the Arctic environment, it was necessary to define a specific Arctic observation dataset. For this purpose, we used the Interactive Training Target toolbox which is a standard tool developed and used for PPS development purposes (introduced by Dybbroe et al., 2004b). It was designed for labelling and analysing selected areas in satellite imagery (denoted *training targets*) and to collect all relevant statistics valid for these selected targets. The collected information concerns the spectral radiances of the target in all available spectral bands but also additional ancillary data. Such ancillary information is e.g. analysed temperature and moisture fields from numerical weather prediction (NWP) models and geophysical information derived from United States Geological Survey (USGS - see www.usgs.gov) datasets.

We have extracted satellite image substets (= training targets) with a size of 5x5 pixels. They were selected over a small area near the Atmospheric Radiation Measurement (ARM) site at Barrow, Alaska (from -177°E to -136°E and 65°N to 76°N) covering parts of the Arctic sea north of Alaska during the period 17th December 2001 to 29th February 2002. The choice of this region is explained by the availability of high-quality and near-continuous cloud observations from cloud radar and cloud lidar instruments at this particular ARM site (not available in any other part at or near the Arctic region at the time of this study). Figure 2 shows the region of interest (denoted *Barrow test area*) as well as other sub-regions of the Inner Arctic which are used later for PPS processing.

A condensed grouping of cloudy targets were utilised here in comparison to the originally defined target labelling. Only three sub-groups were extracted: Cloud-free, Semi-transparent cloudy and Opaque cloudy. In total, 110 cloud-free, 178 semi-transparent cloudy and 130 opaque cloudy training targets were defined over the frozen Arctic Ocean. The land targets (extracted in northern Alaska) amounted to a total of 95 cloud-free, 158 semi-transparent cloudy and 158 opaque cloudy training targets.

The NOAA-15 and NOAA-16 satellites provided the AVHRR data used for this study. They were retrieved at the Comprehensive Large Array-data Stewardship System (CLASS, see http://www.class.noaa.gov/) in Local Area Cover (LAC) format. For defining background datasets of prevailing surface temperatures and vertical profiles of temperature and moisture in the atmosphere, model-analysed data from the ECMWF model (i.e., the ECMWF operational model operated during the time period 17th of December 2001 until 29th of February 2002) were used.

3.2 Overall surface temperature conditions for the studied period

The training targets indicated that prevailing surface temperatures, as approximated by the **T11** brightness temperatures (at the 11 μm spectral channel of AVHRR - nominally called Channel 4) during presumed cloud-free conditions, range from between -51°C to -24°C over land and range from between -45°C to -19°C over the frozen ocean. Importantly, the frozen ocean training targets indicate large surface temperature variations in contrast to the very low surface temperature variations found over the open ice-free ocean, the latter being the intended default conditions for the NS CM test sequence. They also indicate average surface inversions defined

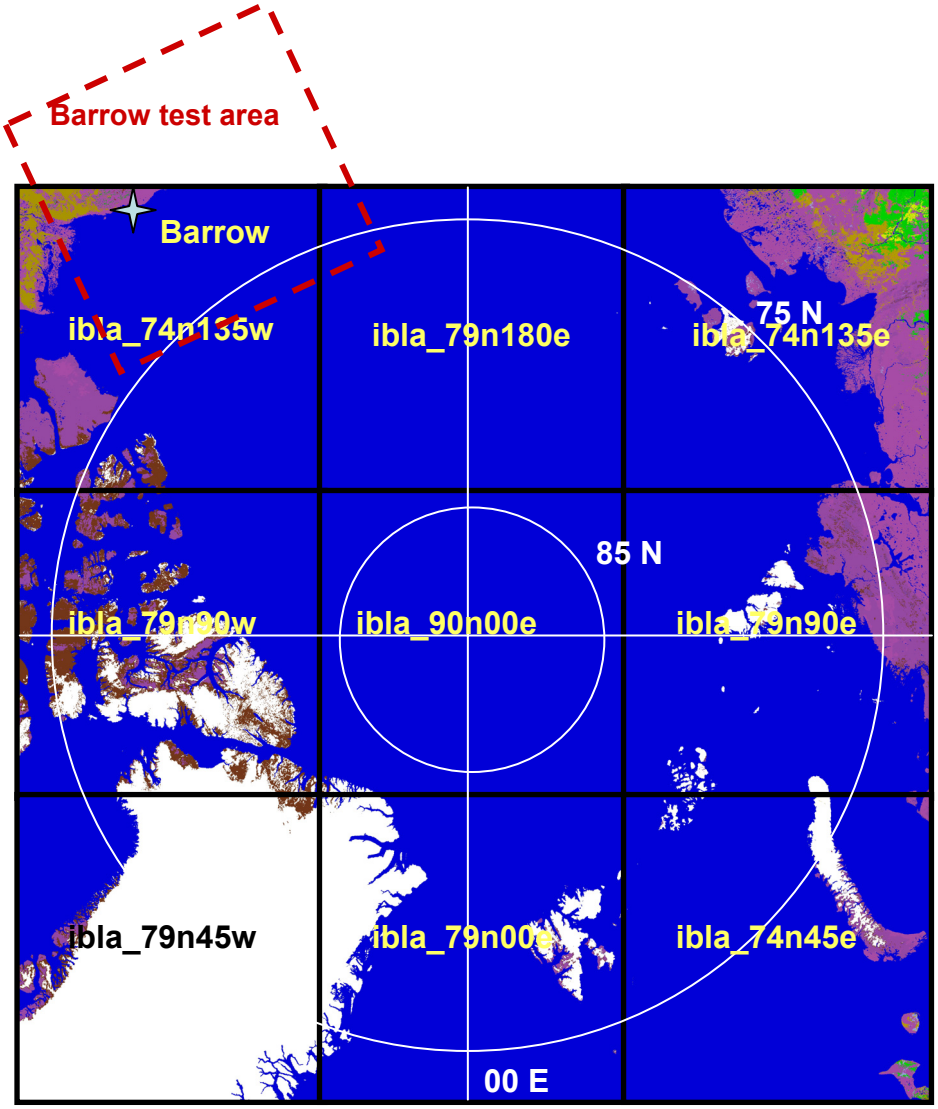

Figure 2. *An overview of the Inner Arctic region and the nine processing areas (or tiles) used for PPS prototyping. Shown is also the Barrow test area which was used for initial target studies.*

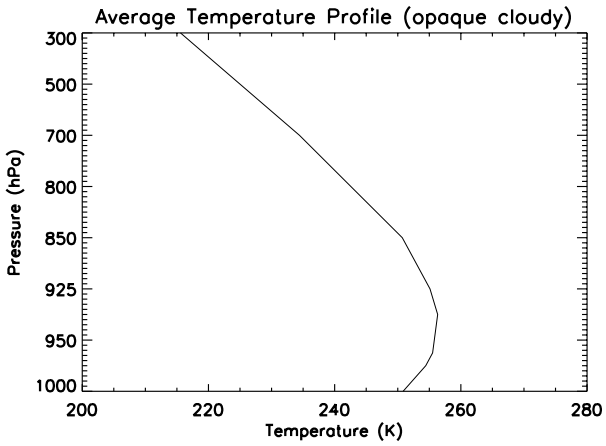

Figure 3. *Average vertical temperature profile computed from the model dataset for all targets labelled as opaque cloudy.*

by the model skin surface temperature (**TS**) minus the model temperature at 950 hPa ($\mathbf{T_{950}}$) of approximately -7K over land and of approximately -6K over the frozen ocean. To illustrate this circumstance Figure 3 shows the average temperature profile from the model dataset for the studied period.
Presumably the most challenging conditions for cloud detection can be found in the pack-ice dominated Arctic winter. Therefore, this will be the main focus of this study.

3.3 Specific studies of the performance of the T11TS feature

Due to the strong dependence on prevailing surface temperature conditions for the success of infrared PPS threshold tests, we will start the illustration of results from training targets by taking a look at conditions for the **T11TS** image feature. Figure 4 shows histograms of the temperature distribution of the **T11TS** values for cloud free (red), semi-transparent cloudy (green) and opaque cloudy (black) training targets over the frozen ocean.

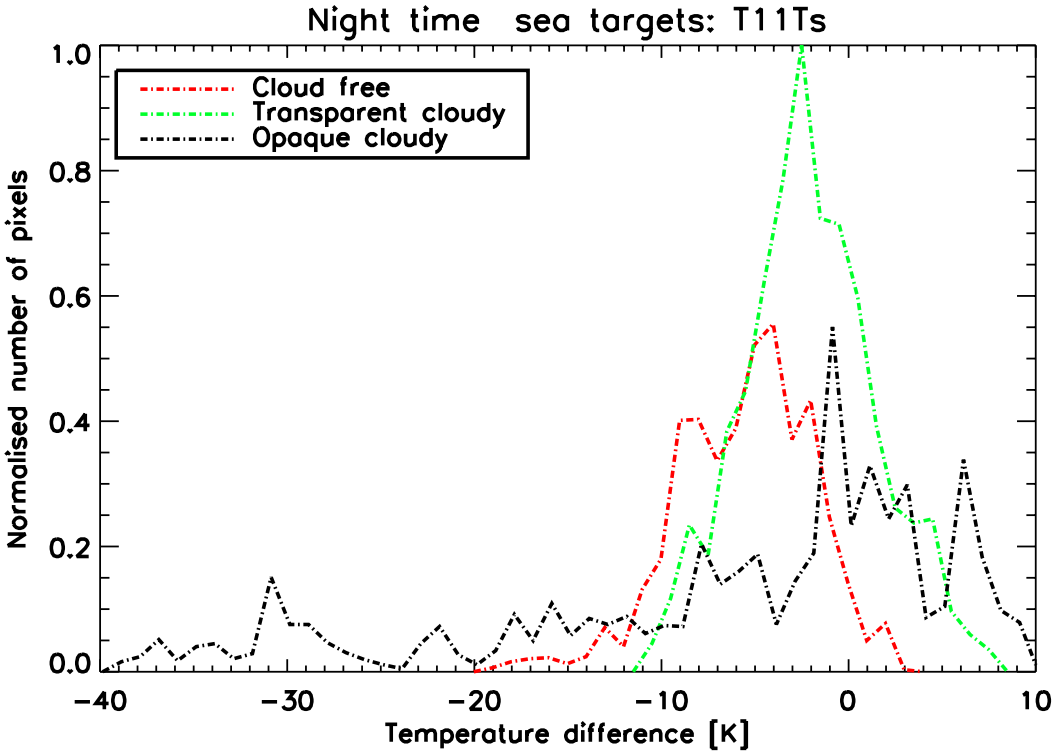

Figure 4. *Histograms of the **T11TS** temperature difference distributions over frozen ocean.*

As indicated in Figure 4, a large portion of the opaque and semi-transparent clouds appear warmer than model-analysed surface temperatures. These relatively warm clouds are probably low clouds trapped under the deep inversion that dominates the Arctic winter. Thin liquid or mixed phased clouds warmer than the surface are quite common in the Arctic during the winter period (Spangenberg et al., 2005). This requires a different approach compared to more traditional image classification approaches to ensure the correct classification of these clouds (to be discussed further in Section 5).

In an attempt to see if we could rearrange the dataset to possibly get an improved separability of cloudy and cloud-free pixels, the training targets were sorted into two **T11TS** groups valid

for extreme and less extreme inversions as seen in Figure 5. The two inversion categories were defined as follows:

Very strong inversions: Below inversion strength defined as $\mathbf{TST_{950}}$ difference < -7 K.

Ordinary inversions: Above inversion strength defined as $\mathbf{TST_{950}}$ difference < -7 K.

Using this sub-division, we will examine the following coarse cloud separation method:

- Assume a pixel to be opaque cloudy if

  T11TS < minimum cloud free **T11TS** pixel value

  or

  T11TS > maximum cloud free **T11TS** pixel value.

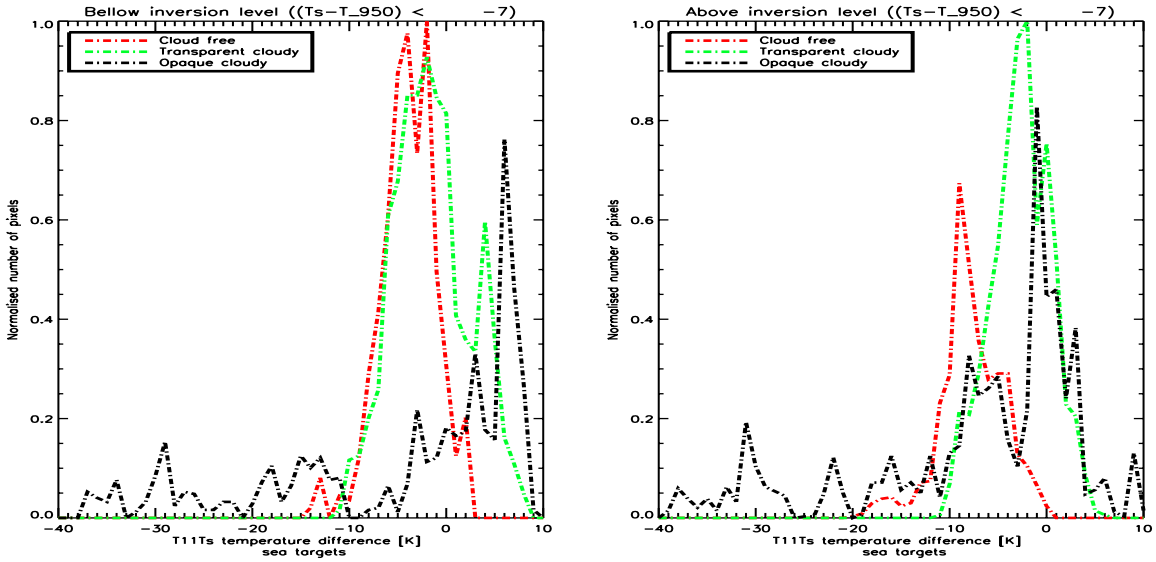

Figure 5. *Histograms of the **T11TS** temperature distributions over frozen ocean after being separated into above **(Very strong, left panel)** and below **(Ordinary, right panel)** an inversion strength defined as $\boldsymbol{TST_{950}}$ < -7 K.*

Table 1 summarises the achieved results from the training targets showing the amount of cloudy pixels which can be distinguished from the cloud free targets using these offsets. The results are separated into:

i) Before the inversion separation (**T11TS**)
ii) After inversion separation (**T11TS_inv**)
iii) 0% misclassifications stands for the ratio of all semi-transparent/opaque clouds captured whilst strictly not misclassifying any cloud free pixels
iv) Whereas 10% misclassifications stands for the ratio of all semi-transparent/opaque clouds captured whilst allowing 5% of the largest T11Ts values and 5% of the lowest T11Ts cloud free pixel values to be misclassified.

Table 1. *The ratio of the total number of cloudy pixels captured before (***T11TS***) and after (***T11TS_inv***) separation into the inversion categories:*

Targets	T11Ts (0% misscl.)	T11Ts (10% misscl.)	T11Ts inv (0% misscl.)	T11Ts inv (10% misscl.)
Semi-transpa	11%	28%	17%	39%
Opaque	37%	60%	50%	74%

The results from Table 1 appear promising since it increases the skill ratio after making the sub-division into the two inversion categories. In the light of these findings it was suggested that the **T11TS** field should be accompanied with a model inversion field for enabling a similar test sequence for PPS. The method used in incorporating such an approach could be to have two sets of offsets, one set used for strong inversion conditions and the second set of offsets to be used on the remaining pixels under less strong inversion conditions. This approach will be further discussed in Section 5.

3.4 Specific studies of the performance of the T37T11 feature

Figures 6 and 7 display the frequency distributions for the **T37T11** feature over ice covered ocean and over land. This feature is normally used in PPS for identification of water clouds and thin Cirrus clouds.

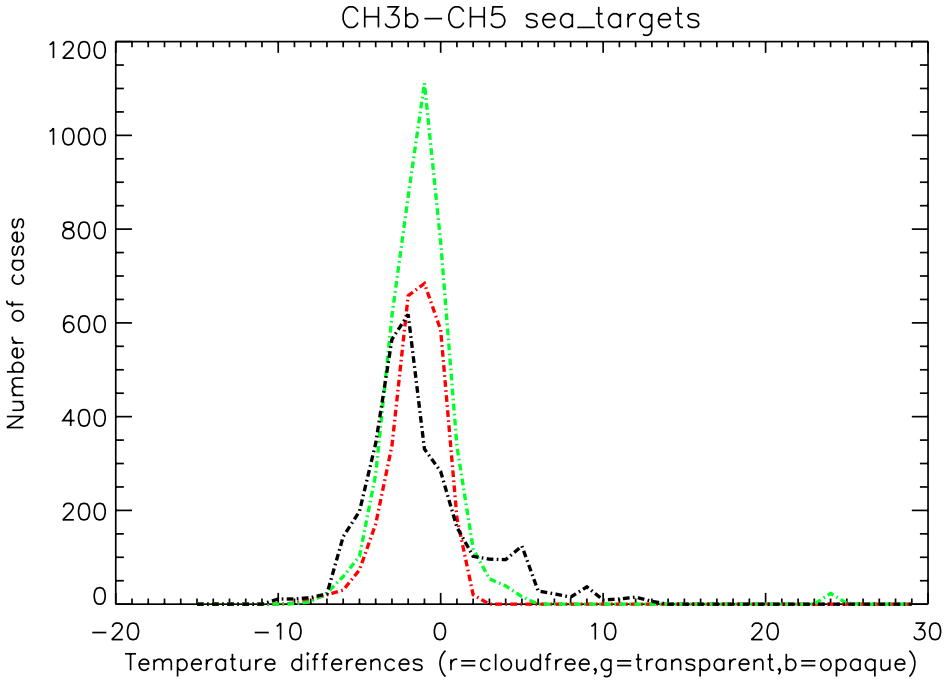

Figure 6. *Frequencies of brightness temperature difference* ***T37T12*** *for training targets over ice-covered ocean (same colour coding as in Figure 5).*

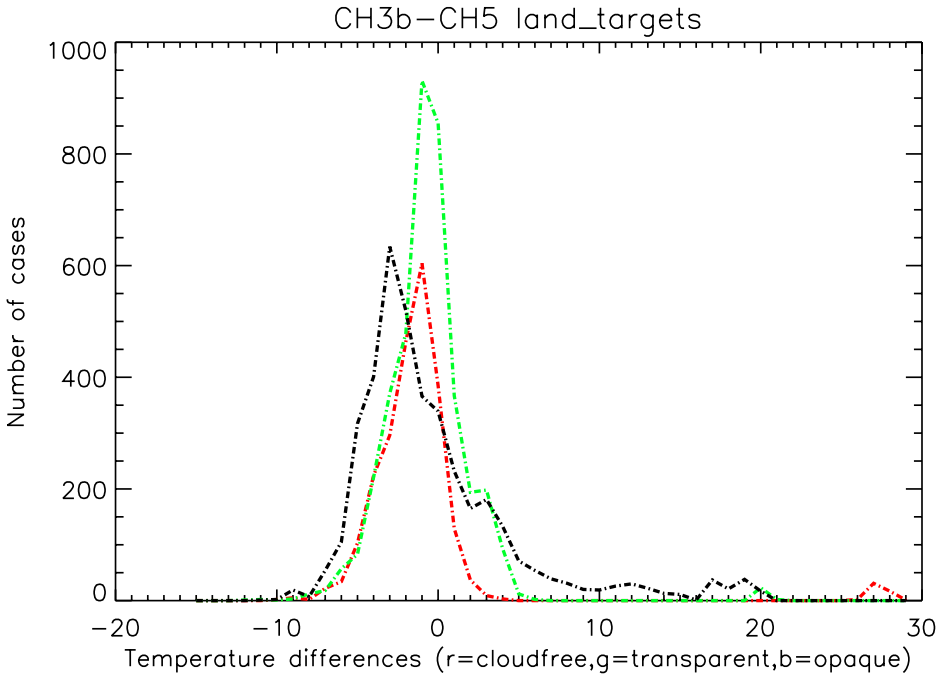

Figure 7. *Frequencies of brightness temperature difference **T37T12** for training targets over land in northern Alaska (same colour coding as in Figure 5).*

We notice a considerable overlap between all three curves indicating a very limited separability between the three categories in the Arctic environment. However, we do see a small tendency for the opaque cloud group to peak towards slightly more negative values indicating some dominance of the typical (i.e., outside of the Arctic region) night-time water-cloud signature. Also, some likely cases of high and semi-transparent (partly mis-labelled targets here) clouds are seen causing high positive differences. Nevertheless, it is clear that it will be very difficult to use this image feature for cloud detection more than for very specific cases and unless further support from other image features can be used in combination with this feature.

3.5 Specific studies of the performance of the T11T12 feature

Figures 8 and 9 display the frequency distributions for the **T11T12** feature over ice covered ocean and over land. This feature is normally used in PPS for identification of thin Cirrus clouds (showing a positive difference for these clouds in a normal atmosphere).

Interestingly, we cannot see any sign of the "normal" positive temperature difference that is commonly seen in areas outside of the Arctic for semi-transparent clouds. Again, we conclude that also here it will be very difficult to use this image feature for cloud detection more than for very specific cases and unless further support from other image features can be used in combination with this feature.

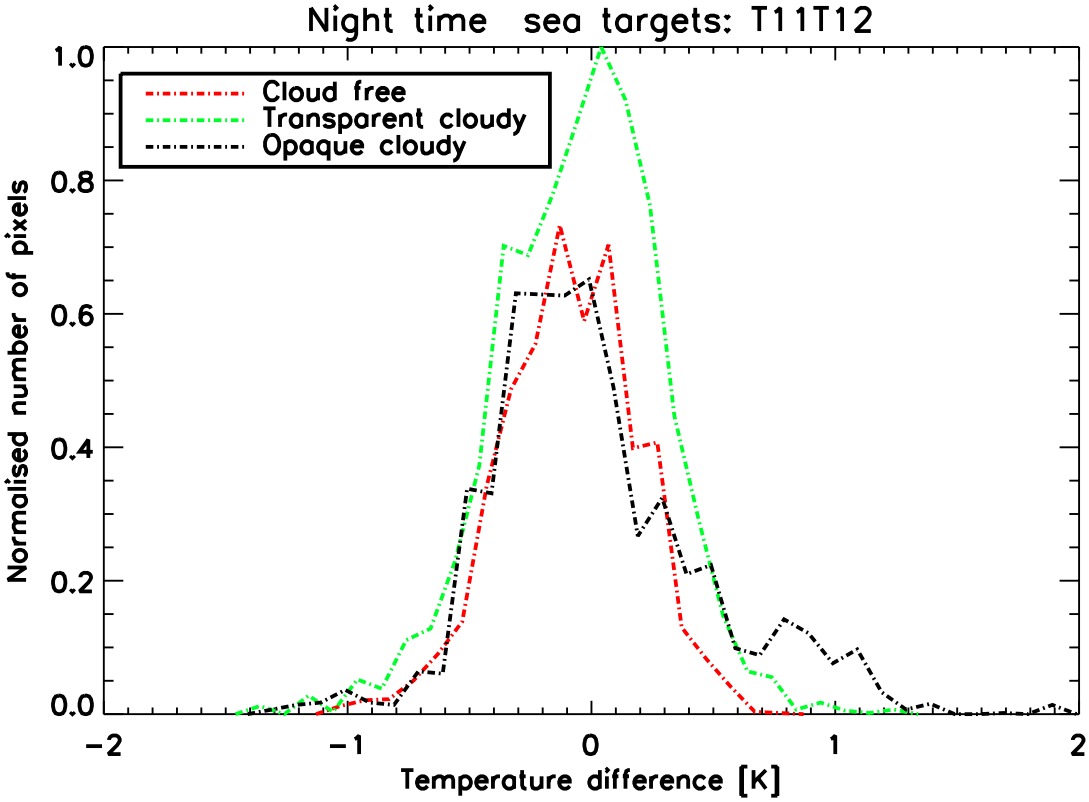

Figure 8. *Frequencies of brightness temperature difference **T11T12** for training targets over ice-covered ocean.*

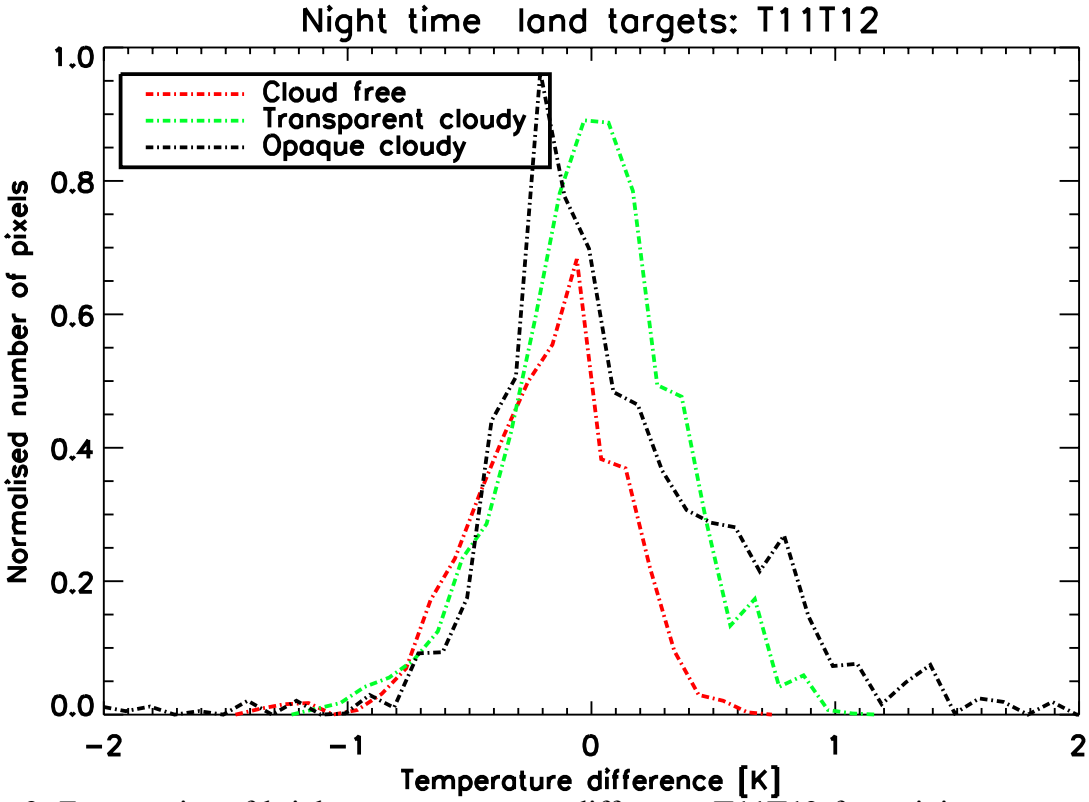

Figure 9. Frequencies of brightness temperature difference **T11T12** for training targets over land in northern Alaska (same colour coding as in Figure 8).

Assessing model-analysed surface temperatures and the need for atmospheric corrections of PPS thresholds

The training targets were not solely selected to quantitatively validate the revised test sequences, but also to assess to what degree an atmospheric correction is needed to correct the outgoing long wave radiances. The satellite-measured long wave radiances are different from the originally emitted radiances at the Earth's surface and from clouds due to absorption and reemission processes by water vapour and other gases in the atmosphere with temperatures different from the surface temperatures. Usually water vapour (the dominating emitting/absorbing gas at the studied wavelengths) is colder than the surface, therefore the remotely sensed radiances are somewhat diminished in comparison to the true surface radiances. The need for an atmospheric correction increases for increasing water vapour content and increasing satellite zenith angles. The expected effect in a standard atmosphere (i.e., with monotonously decreasing temperatures with altitude in the troposphere) is an increased negative **T11TS** bias for an increased amount of water vapour in the atmosphere, especially in combination with large satellite zenith angles (giving a long path-length through the atmosphere for the measurement).

A way to estimate the importance of such atmospheric corrections is to study how satellite-measurements of **T11** compares to model-analysed **TS** temperatures (for the moment assuming that model-analysed values are reliable). Figure 10 shows the model column water vapour (WV) of the cloud free training targets plotted against the corresponding **T11TS** feature (i.e., measured brightness temperature as a function of model-analysed surface temperature) values for sea targets (top) and land targets (bottom). In addition, Figure 11 shows the satellite zenith angle of the same cloud free training targets plotted against the corresponding **T11TS** values.

Figure 10 shows no indication of decreasing **T11TS** values for increasing WV values. Furthermore, Figure 11 does not show any indication of decreasing **T11TS** values for increasing satellite zenith angles. The **T11TS** tests' dependency on WV and satellite zenith angles appears, at most rather small which indicates little or no need for an atmospheric correction.

This could be due to several factors. Firstly, for a completely dry atmosphere the expected **T11TS** bias should be zero for cloud free pixels (if assuming that water vapour is the only emitting/absorbing gas of interest at this wavelength). The training targets show very low WV values, generally in the range of 0.8-2.5 kg/m^2, which indicates a very dry atmosphere. Secondly, in extreme inversion situations such as the conditions found during the Arctic winter, the usual relationship between **T11TS** and model column water vapour may be reversed (i.e. tend towards a positive bias for higher values). The strong inversion conditions that dominate the Arctic winter may result in that the water vapour, predominately found close to the Earth's surface, tends to radiate at higher temperatures than the surface temperature. This will instead cause the difference **T11TS** to shift towards a positive temperature bias as a function of increasing WV values and more so for the strongest surface inversions.

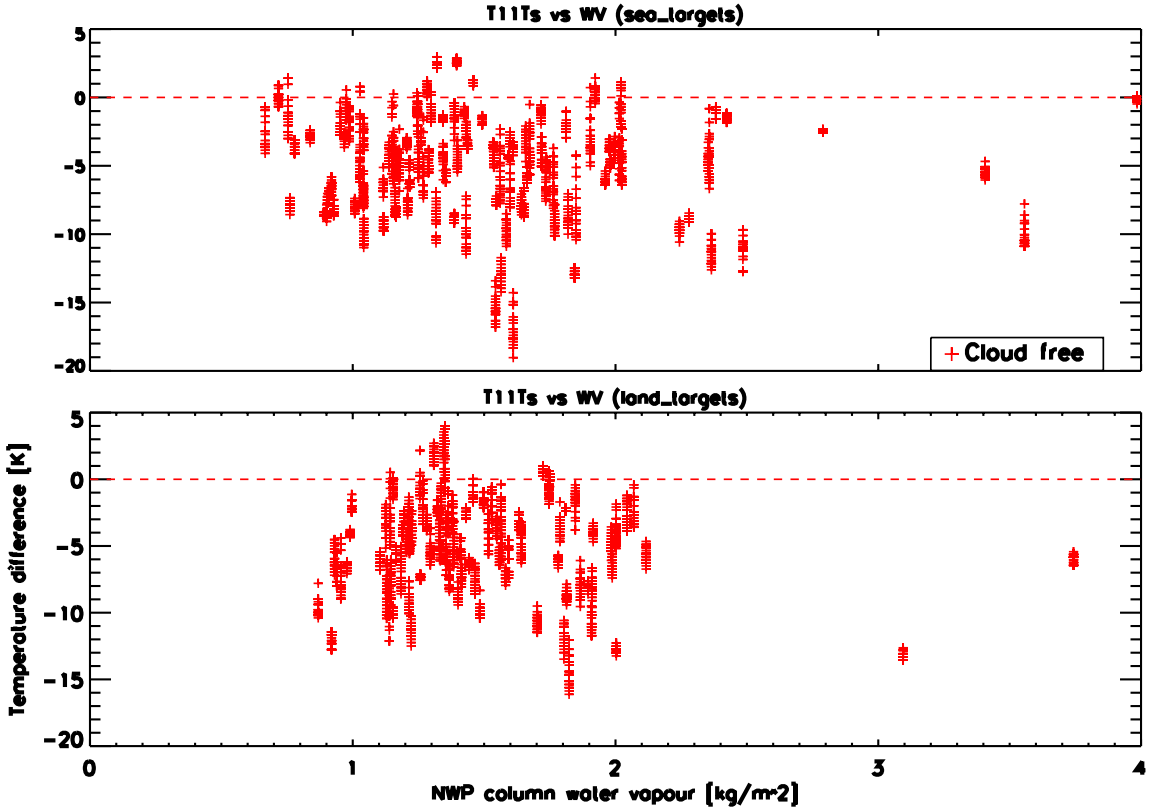

Figure 10. ***T11TS*** *as a function of model column integrated water content for cloud free targets over ice-covered ocean north of Alaska (top) and over land in northern Alaska (bottom).*

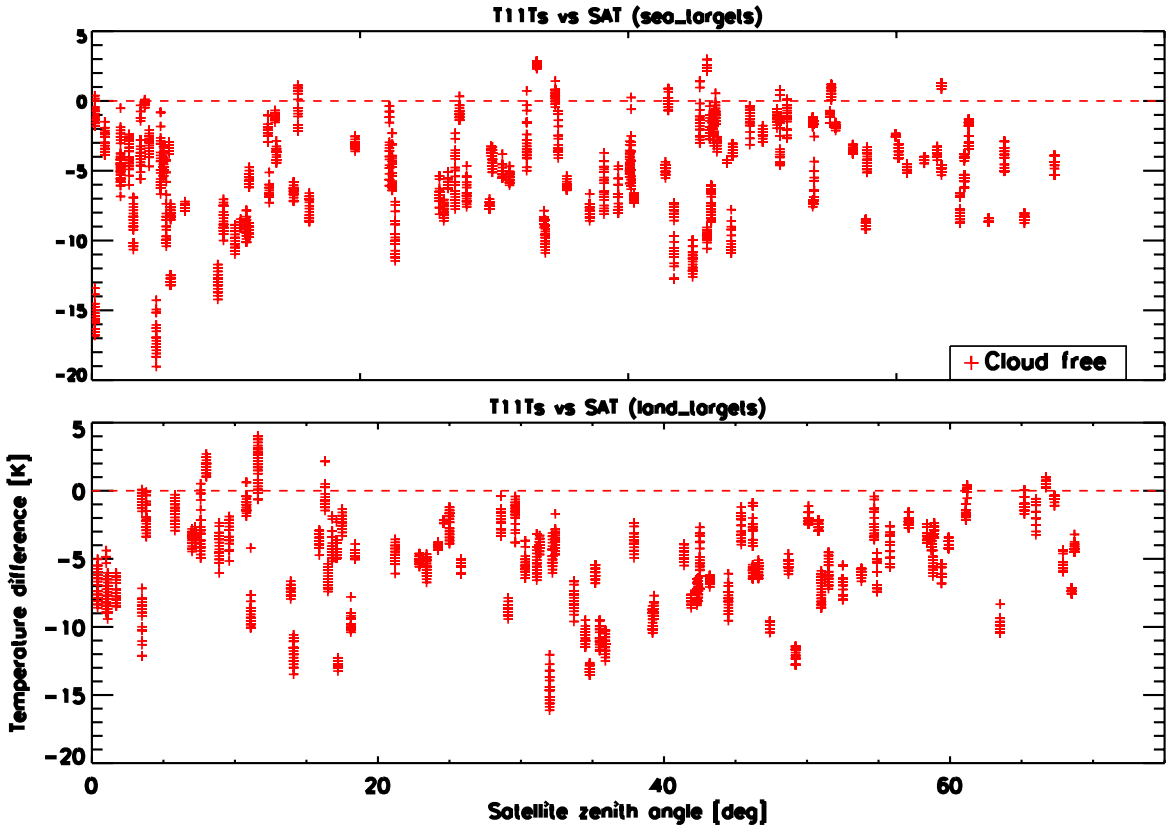

Figure 11. ***T11TS*** *as a function of satellite zenith angle for cloud free targets over ice-covered ocean north of Alaska (top) and over northern Alaska (bottom).*

Figure 12a (sea ice targets) and 12b (land targets) show 2-dimensional histograms of the **T11TS** tests' dependency on both inversion strength and WV during cloud free conditions at low satellite zenith angles ($\alpha \leq 60°$). Here inversion strength is defined as the model surface temperature minus the model temperature at 925hPa.

Figures 12a and 12b appear to indicate a tendency of increasing (towards positive) **T11TS** values for stronger inversions and more prominently for an increased amount of WV. This indicates that the strong surface inversions in the Arctic do in fact cause the T11TS bias to tend towards positive values. Also take into consideration that the temperature analyses used here are heavily influenced by short model predictions (normally 6-hour forecasts) due to a lack of real surface observations and which may have difficulties predicting very strong surface inversions. We may consequently conclude that if model analyses had been more realistic the trends towards more positive **T11TS** values would have been even more pronounced than what is shown by Figures 12a and 12b. However, a more comprehensive study would be needed to assess the true nature of the varying **T11TS** values as a function of WV and surface inversion strength.

One very clear feature of the studied dataset in the Arctic region appears to be the robust negative **T11TS** bias of around 5K for cloud free targets, i.e. the model surface temperature is 5K too warm. This bias can be clearly seen in the previous Figures 10 and 11. It is attributed to model skin surface temperature errors which almost always overestimate the surface temperature in the Arctic.

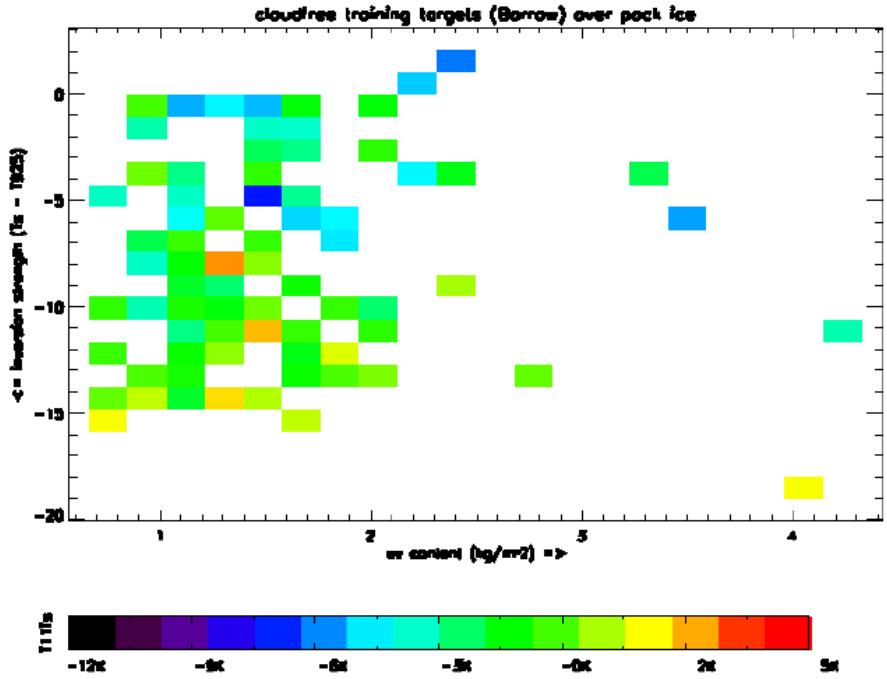

Figure 12a. *Two-dimensional histogram of **T11TS** (colour categories) as a function of model column integrated water vapour and model inversion strength for targets over ice-covered ocean north of Alaska.*

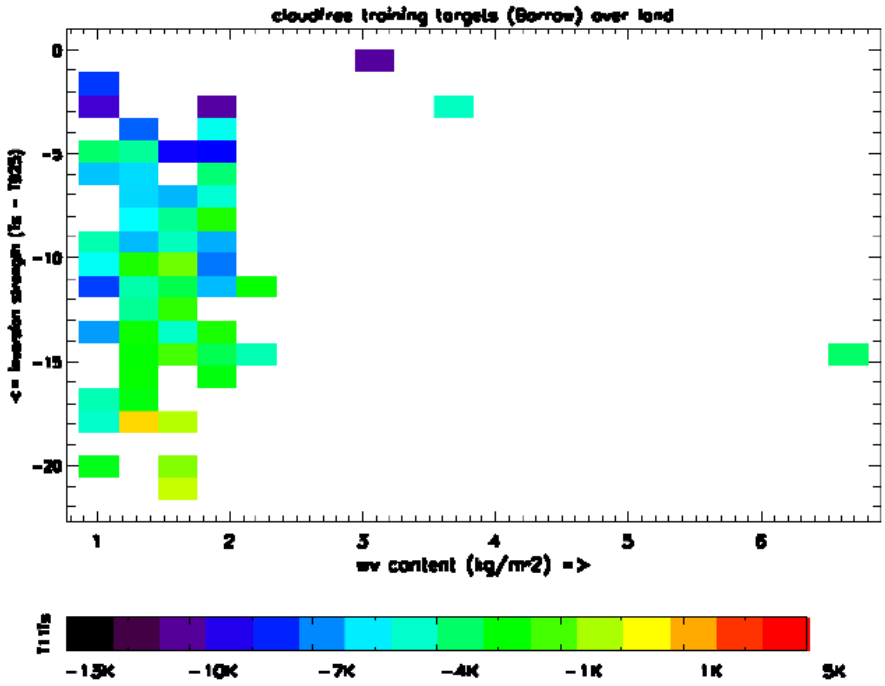

Figure 12b. *Two-dimensional histogram of **T11TS** (colour categories) as a function of model column integrated water vapour and model inversion strength for targets over land in northern Alaska.*

Figure 13 below shows the difference **T11TS** as a function of time for sea targets (top) and land targets (bottom).

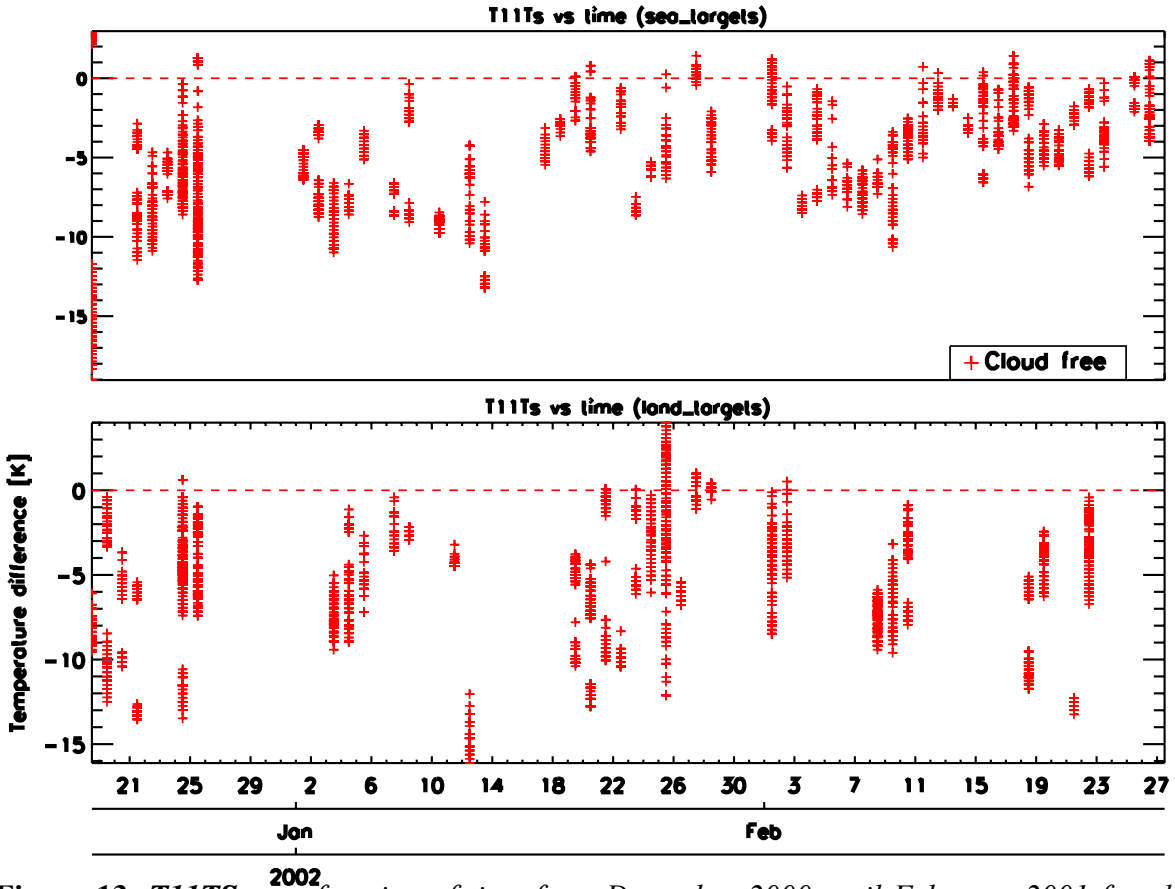

Figure 13. ***T11TS*** *as a function of time from December 2000 until February 2001 for cloud free targets over ice-covered ocean north of Alaska (top) and for land targets in northern Alaska (bottom).*

The seasonal bias of **T11TS** is remarkable, ranging from around -8 K in mid winter to -4 K by the end of February. To examine the causes of this gradually changing bias that is experienced over the Arctic Ocean is not a part of this study. We may speculate that the decreasing frequency of cases with very strong surface temperature inversions which takes place when approaching springtime conditions could reduce the experienced bias of analysed and/or modelled surface temperatures. In any case, the large bias during the polar winter certainly causes some problems when defining suitable thresholds and offsets for the Cloud Mask (CM) test sequence wherever the **T11TS** test is used.

3.6 Specific studies of the performance of texture features

The texture feature uses a field of variances where every pixel in a scene has been assigned a variance value. The variance of each pixel is derived from the standard deviation of 25 pixel values from the pixel at hand and the surrounding 24 pixels.

In test 3 in the NS CM test sequence v1.6 (see Section 2), pixels with variances values larger 0.9K for **T11_text** (variance of **T11**) and 1K for **T37T12_text** (variance of the **T37T12** test) are considered partially cloudy (CM value=2). This makes sense over open ocean areas which

are very homogenous, but this relationship is not useful for ice-covered oceans. The pack ice of the Arctic contains many cracks, often with open water protruding to the surface (leads) and ridges. These cracks, leads and ridges contribute to high to very high surface texture values. Figure 14 shows the histogram distribution of target **T11_text** values for targets over ice-covered ocean.

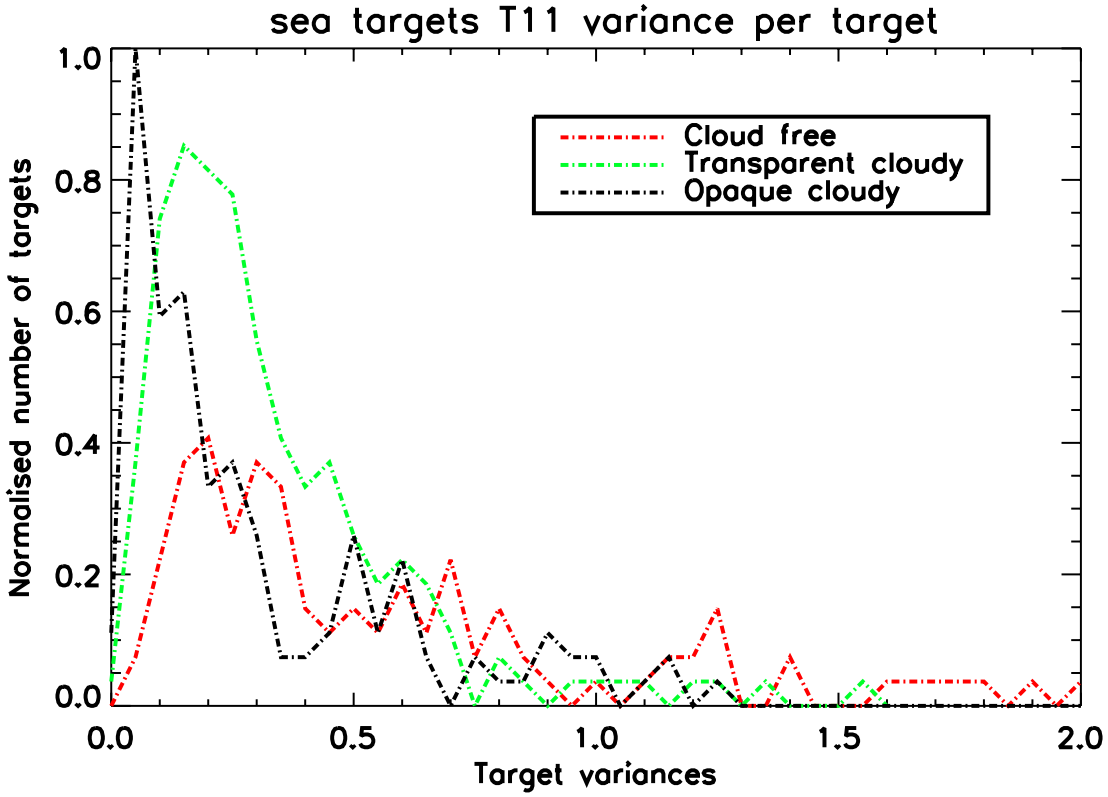

Figure 14. *Histogram distributions of the target **T11** variances **(T11_text)** over the frozen Arctic Ocean.*

Obviously (if comparing threshold values to results in Figure 14), over the Arctic the high variance of the crack, lead and ridge covered pack ice causes test 3 in the NS CM v1.6 to misclassify most cracks, leads and ridges as partially cloudy. Some sub-pixel and semi-transparent clouds may still be attained here, but this test should not be used in the same manner as in the NS CM because of the significant misclassification of cloud free areas. On the other hand there may be a real potential for using the aforementioned texture feature to detect cloudy pixels with low variance values. When combined with certain temperature tests presented later in Section 5, the new CM can thus be further strengthened.

The second texture feature used in NS CM is **T37T12_text**. Figure 15 shows the histogram distribution of the target **T37T12_text** values for the frozen Arctic Ocean.

This texture feature shows a similar signal and could to some extent be used in combination with other tests to find cloudy pixels with low variances (discussed further in Section 5).

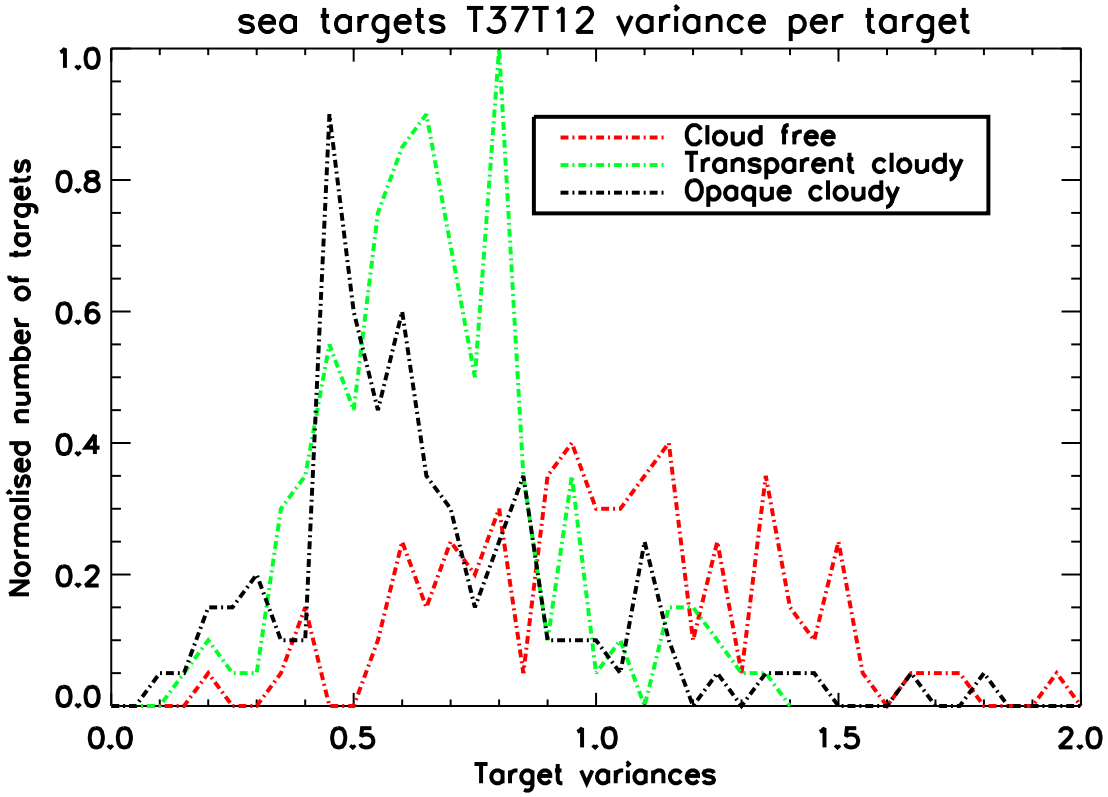

Figure 15. *Histogram distributions of the target **T37T12** variances over the frozen Arctic Ocean.*

4 PPS Night Sea (NS) CM results on training targets

After having studied in general the conditions that are met in typical Arctic polar night situations, we are now ready to examine more in detail the performance of the current standard PPS CM algorithm when facing such conditions. One easy way of doing this is to process PPS using the information stored for every training target and to examine the results compared to the original labelling of each training target (the method demonstrated by Dybbroe et al., 2004b).

However, before presenting any results we have to claim that a direct use on the training targets of the current NS CM test sequence as presented in Section 2 is practically meaningless. The reason is that it is clear that it will fail almost to 100 % (see also results later in Section 6 and Figure 24) during the Arctic winter due to one particular and fatal test; Test number 7 (see Section 2). Clearly, NS CM v1.6 is not suitable for Arctic conditions.

Also, recall from section 2 that

1) NS CM v1.6 will not classify any clouds as being opaque since test 1 overrides test 4 (i.e., they have the same **T11T37** threshold).
2) Tests 5 and 6 don't work during the Arctic winter since **TS** is generally below 273K.

A more fair evaluation of the current PPS algorithm would consequently be to examine results without using the fatal test 7. After all, test 7 was added for specific reasons that were not particularly addressing the task of correctly identifying clouds but rather the task of correctly identifying cloud-free and ice-free sea surfaces. Consequently, a corresponding alternative

version of PPS NS CM was created. This test sequence had the same setup as the official NS v1.6 but it did not include test 7. Furthermore, tests 4 and 5 were placed at the beginning of the test sequence for favouring the early identification of opaque cloudy pixels. In the following, we will call this version ~v1.4 (since it resembles very much the previous version v1.4).
The following results were now achieved:

Cloud-free targets: 53 % correctly classified
Semi-transparent cloudy targets: 38 % correctly classified (1 % Opaque cloudy)
Opaque cloudy targets: 4 % correctly classified (63 % Semi-transparent cloudy)

An alternative presentation of results only concentrating on the performance of the binary value Cloud Mask (i.e., Cloudy or Cloud-free) yields:

Cloud-free: 53 % correct
Cloudy: 51 % correct

Although it is difficult to assess to what degree the selected training targets are really representative, the results achieved here appear quite poor (almost 50 % of the pixels are wrongly classified). This was somewhat expected prompting the creation of a new test sequence to be mainly used during the Arctic winter. Another important shortcoming in assessing the skill of the NS CM along with the creation of an improved Arctic Cloud Mask is the poor quality of the PPS dynamical thresholds in Arctic conditions, as these thresholds perform poorly in very cold and very dry conditions. This is discussed in more detail in Section 7.

Results from the training target studies presented in Section 3 gave an early indication of which tests were likely to be efficient or inefficient in a test sequence applied to Arctic winter conditions. The current CM performs poorly over the Arctic partly due to the very cold surface temperatures, persistent strong surface inversions and a strong sensitivity to cracks in the pack ice (leads). The last feature is especially serious for the use of spatial homogeneity tests (here local texture tests) and all Cirrus detection tests (see section 5.3).

It should also be noted that the cold surface temperatures and the associated warmer (relative to the surface) lower tropospheric layers leads to seriously reduced efficiency of traditional temperature difference features such as **T37T12** and **T11T12**. Notice, however, the possibility to instead utilise inverted temperature differences in the Arctic area (further elaborated in Section 5).

5 Creation of a new Ice Night Sea (INS) test sequence

5.1 Basic ideas for a modified Cloud Mask method

The first step in the modification of the test sequence was to remove any restrictions due to specific modelled surface temperatures. The idea was to create a new test sequence based on the Special Sensor Microwave Imager (SSM/I) derived ice maps from Ocean Sea Ice Satellite Application Facility (OSISAF). The revised CM was to be utilised only if the surface consisted of sea ice, as is usually the case during Arctic winter. To assist in choosing which direction to take for the new Ice Night Sea (INS) CM test sequence, histogram temperature distributions of all of the tests included in the current NS test sequence were analyzed further. At first glance the **T11T12**, **T11T37** and **T37T12** tests appeared relatively fruitless (already commented in

Section 3). The **T11TS** and the T11 texture (**T11_text**) tests however, showed some potential and hence inspired the direction taken for the new test sequence.

Some initial ideas concerning whether it was possible to use the NWP model information to derive strong or weak inversion surface inversions (briefly mentioned in section 3.3) also materialized from studying the various fields contained in the training targets. The idea was that the provided model atmospheric profile can be used in the existing CM method but instead using 2 sets of static offsets for all T11Ts tests in the test sequence. One of the aforementioned static offsets would be applied during extreme inversion conditions and the other static offset would be used under less extreme inversions. Using this method should not change the rate of cloud free pixel misclassifications as the offsets are chosen specifically not to misclassify cloud free pixels. Early results based on training targets indicate that this approach may be more promising over land.

Unfortunately, preliminary evaluations of the use of inversion fields on entire regions show that the inversion feature is not as useful for the new Ice Night Sea Cloud Mask as the training targets indicated, and work regarding the use of model surface inversions was halted. The use of model surface inversions should still be considered, but this would be have to be part of a future study.

Further development and evaluation of results required testing the CM test sequence on 1250 x 1250 pixel regions (scenes). It was tested on approximately 100 scenes in total entire scenes covering the entire Arctic region. The new INS CM was consequently applied and tuned to scenes of the entire Arctic area for January 2007 and, in addition , around 50 scenes covering the Central Arctic north of Alaska from the winter December 2001 to March 2002 (Barrow region). These scenes contained a large number meteorological scenarios and surface conditions which put the test sequence to a test. It also gave a first impression of how the PPS CM (for land) works for the extreme conditions prevailing over Greenland.

5.2 The finally proposed INS CM test sequence

Following is a brief overview of the resulting final test sequence (and its static offsets) of the proposed INS CM. The following test sequence includes quality margins for each test, i.e. for test 2 if a pixel has its **T11TS** value less than -17 K minus a quality margin then the pixel is cloudy with ‘certainty’ and is flagged ‘good quality’. The test sequence is then halted for the pixel at hand and thereafter the test sequence is restarted on the next pixel. Whereas if a pixel has a T11TS value between -17 K minus a quality margin and -17 K then the pixel is probably filled with a cold cloud but is flagged as ‘poor quality’. If a pixel is flagged "poor quality" the test sequence continues until the pixel is flagged "good quality" or the end of the test sequence is reached. Also note that all tests in the test sequence, except the variance features include the PPS dynamical thresholds derived from the RTTOV radiative transfer model. All static offsets are in Kelvin units.

Shown below is the new INS CM test sequence (to be compared to the original NS CM test sequence described in Section 2):

Ice Night Sea Cloud Mask (INS CM)

---

1) **Water clouds (**CM = 3**)** if **T11T37 > 0.5 K & T37T12_text < 0.6 K**

2) **Cold clouds** (CM = 3) if **T11Ts < -18 K**

3) **Semi-transparent Cirrus** (CM = 2) if **T37T12 > 1.9 K & T37_text < 1.9 K**

4) **Thin water clouds** (CM = 2) if **T37T12 < -1.6 K & T37T12_text < 0.6 K**

5) **Warm clouds** (CM = 3) if **T11Ts > 3 K & T11T37 > 0.3 K & T37T12 < -0.4 K & T37T12_text < 0.6 K**

6) **Warm semi-transparent clouds** (CM = 2) if **T11T12 < -0.7 K**

7) **Extra ice cloud test (**CM = 2**)** if **T11T12 > 0.7 K & T37_text < 1.9 K**

8) **Extra water cloud test** (CM = 3) if **T11T37 > 2 K**

Prerequisites:

Should the strong positive bias of the model surface temperature be rectified and/or the resolution and precision of the dynamical thresholds be enhanced, then the static offsets presented here will need adjusting accordingly. Also note that leads and pixels containing a mixture of ice and open water exhibit large temperature differences in, for instance, the **T37T12** test which is typically used to detect Cirrus during night conditions.

The use of the Planck function to convert measured digital counts (with a linear relation to radiances due to sensor characteristics) to equivalent brightness temperatures means that we have a strongly non-linear relation between digital counts and brightness temperatures, especially at shorter wave lengths such as in the AVHRR channel at 3.7 micron (**T37**). Therefore, when individual pixels exhibit large sub-pixel scale temperature differences, the warmer radiance contributions dominate over the cooler radiance contributions and the total radiance of the pixel is therefore biased towards the warmer contribution. This is true for all wavelengths but the effect is much weaker for longer wavelengths such as at **T12**. Pixels that contain a combination of open water, at around 270K and pack ice, at around 240K, typically because of the presence of leads, are extreme cases of this situation in the Arctic environment.

5.3 The use of local texture features

There are two texture features included in the INS CM, the **T37T12_text** and **T37_text** features.

The **T37T12_text** feature can be used as a simple noise filter. At very low temperatures the radiance measured at 3.7 μm wavelength (**T37**) has a very low signal-to-noise ratio, importantly, more so than **T12**. This is a result of the relation between digital counts and brightness temperatures (mentioned earlier) and that the AVHRR sensor must be capable of measuring higher radiances at 3.7 μm wavelength than at other infrared wavelengths (due to additional reflected solar radiation during daytime in this channel). In areas with significant noise in **T37**, the variance (texture) of the **T37T12** test is high. The high **T37T12_text** values can be explained by 'noisy' **T37** radiances minus 'less noisy' **T12** radiances giving rise to a noise enhanced or reduced temperature difference, often varying from pixel to nearby pixel. It was empirically derived that using a static offset of **T37T12_text** < 0.6 K accompanied with all water cloud and semi-transparent clouds (warm in relation to the surface) tests it was possible to significantly reduce the misclassification of certain cloud free areas as cloudy. However, using the **T37T12_text** feature in this manner inevitably weakens the cloud masks ability to detect clouds with high textures. Nevertheless, the 'clouds lost' to 'reduced cloud free misclassifications' ratio appears low and therefore warrants this approach.

The **T37_text** feature is used in the tests aimed to detect clouds with high variance values such as semi-transparent ice clouds. This texture feature is necessary because of the presence of leads and ice contaminated ocean. These can be seen through their very large positive **T37T12** values, which are often larger than the typical signature of semi-transparent Cirrus. Leads are, however quite local compared to Cirrus; hence the variance at **T37** is quite large in the vicinity of leads. It was empirically derived that using a static offset of **T37_text** < 1.9 K accompanied with Cirrus tests is sufficient to avoid misclassifying leads as Cirrus. The better performance of the **T37_text** feature here instead of the **T37T12_text** feature is suggested to be an effect of the fact that we have a higher atmospheric transmissivity at 3.7 μm, thus favouring the observation of surface features compared to atmospheric features.

Figure 16 shows a representative RGB scene from Barrow (top – see Barrow test area definition in Figure 2) and the **T37T12_text** feature for the same scene (bottom left) and the difference between **T37T12_text** and **T37_text** (bottom right). This figure illustrates that the **T37_text** feature is more suitable for identification of ice cracks or leads than the **T37T12_text** feature. For example, the ice cracks in the northern part of the region are more or less invisible in the lower left panel of Figure 16 while they are clearly visible if subtracting the **T37_text** feature (lower right panel of Figure 16).

The upper portion of the **T37T12_text** scene (bottom left) is very cold and **T37** has a very low signal-to-noise ratio there. This can also be seen by the relatively high **T37T12_text** values in that area. To some degree the leads can be seen as light coloured 'strips'. In the bottom right figure it can be clearly seen that, in the vicinity of leads, the **T37_text** feature has a considerably higher variance than what can be seen in the **T37T12_text** feature. Leads along with other areas where the pixels are highly affected by the non-linearity mentioned earlier are clearly visible by contrast between the two features (dark areas/lines). Figure 17 shows a representative RGB scene from a region surrounding Svalbard (top) and the **T37T12_text** feature for the same scene (bottom left) and the difference between **T37T12_text** and **T37_text** (bottom right).

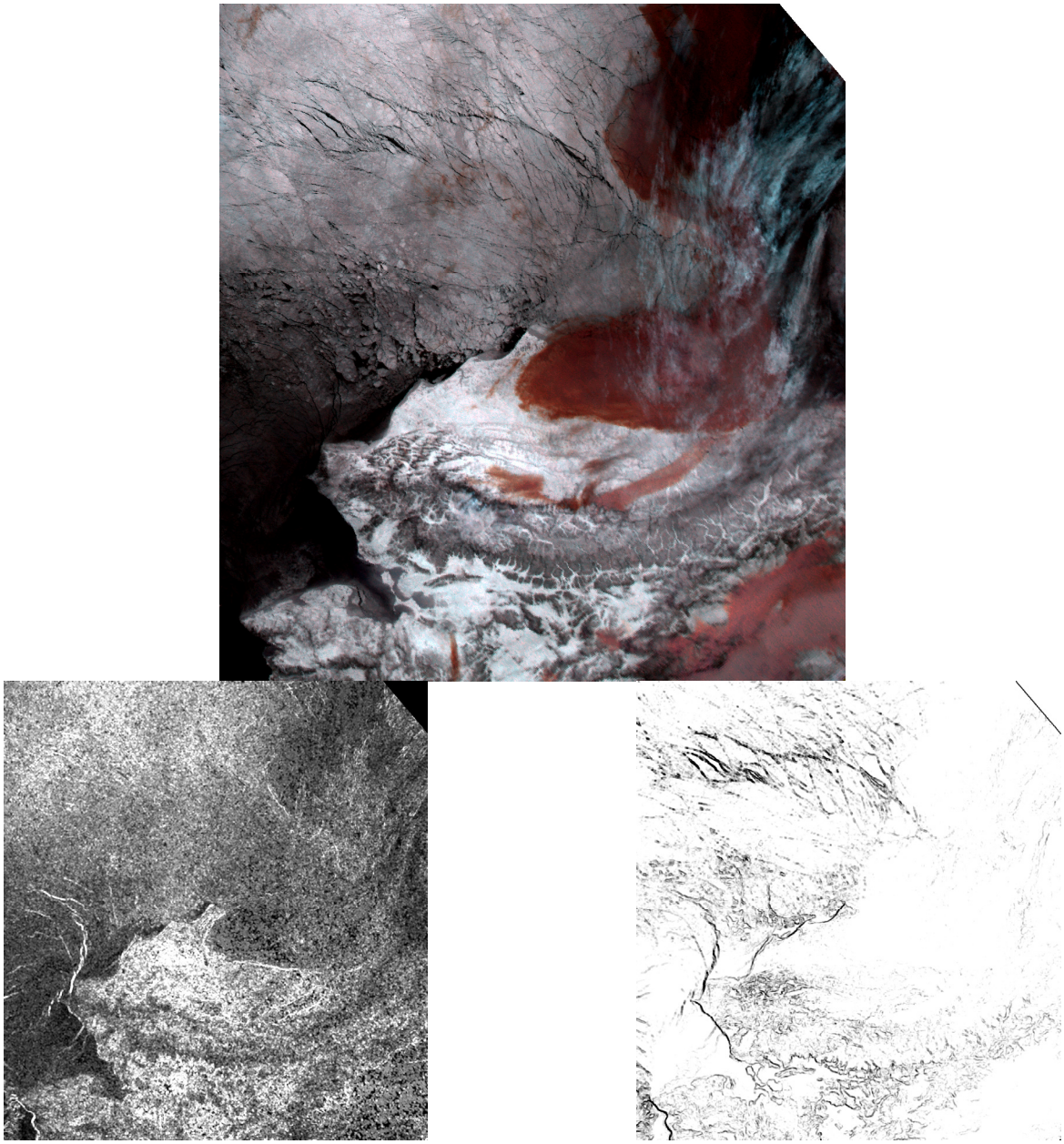

Figure 16. *An RGB scene from NOAA-17 of the Barrow region from 18 December 2001 at 15:40 UTC (top), the corresponding* ***T37T12_text*** *feature (bottom left) and the* ***T37T12_text*** *minus* ***T37_text*** *difference (bottom right). For the RGB scene, light areas are colder than dark areas, Cirrus clouds appear blue and Stratus and semi-transparent low clouds appear brown coloured. For the bottom figures, dark areas have lower values than light areas.*

Svalbard can be clearly seen in the east and eastern Greenland can be seen in the northwest of the scene. Figure 17 also shows that the leads appear more visible in the **T37_text** feature (bottom right). Notice also how clearly visible the coast of Svalbard and the area of mixed ice and water north of Svalbard are. This is due to the large temperature differences within the pixels. Cold areas containing noise have somewhat elevated values in the **T37T12_text** feature.

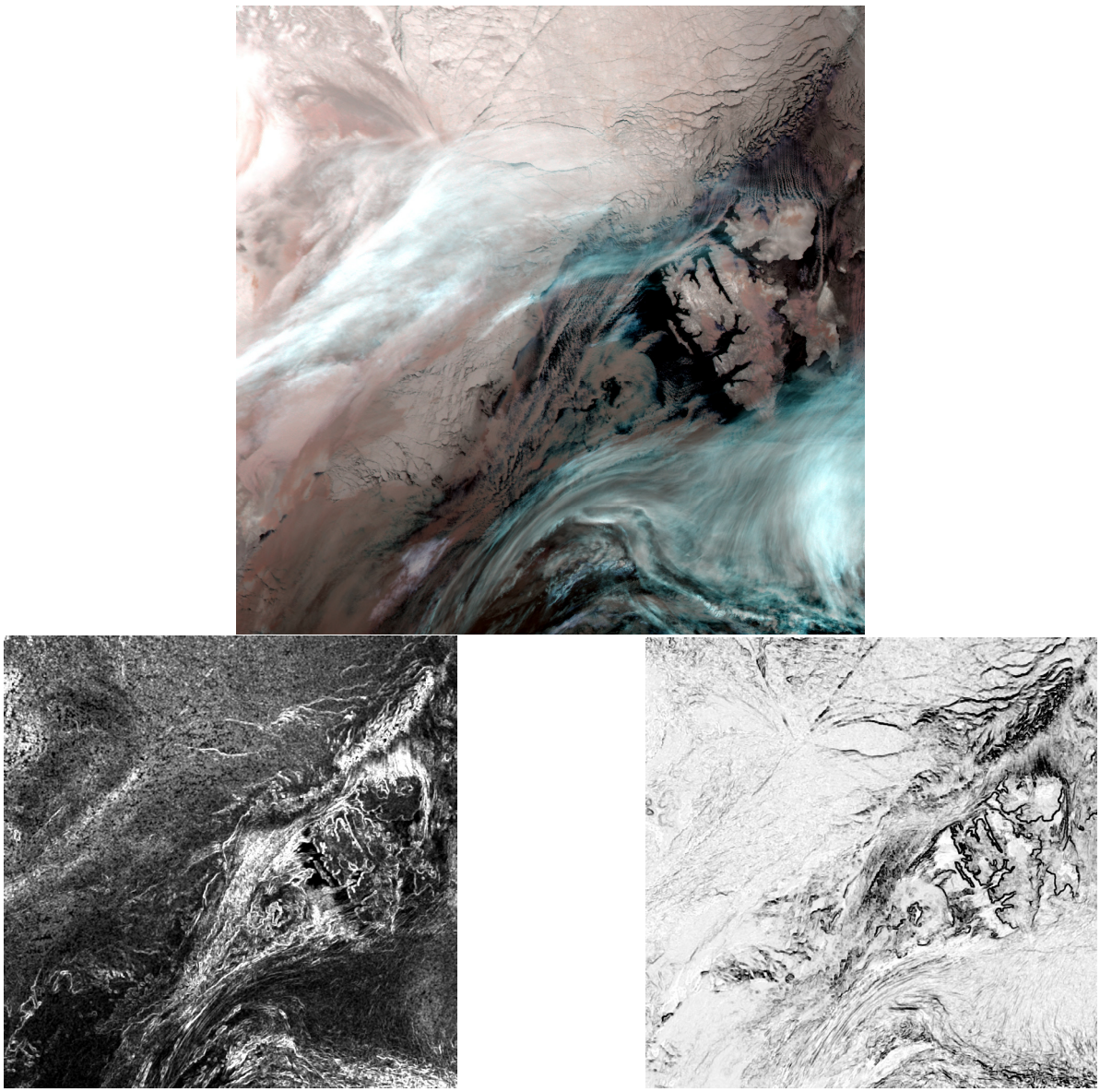

Figure 17. *An RGB scene from NOAA-18 of the Svalbard region (tile ibla_79n00e in Figure 2) from 1st of January 2007 at 03:14 UTC (top), the corresponding* ***T37T12_text*** *feature (bottom left) and the* ***T37T12_text*** *minus* ***T37_text*** *difference (bottom right).For the RGB scene, light areas are colder than dark areas, Cirrus is blue and Stratus and semi-transparent low clouds are brown coloured. For the bottom figures, dark areas have lower values than light areas.*

Figure 18 shows a representative RGB scene from Greenland (top) and the **T37T12_text** feature for the same scene (bottom left) and the difference between **T37T12_text** and **T37_text** (bottom right).

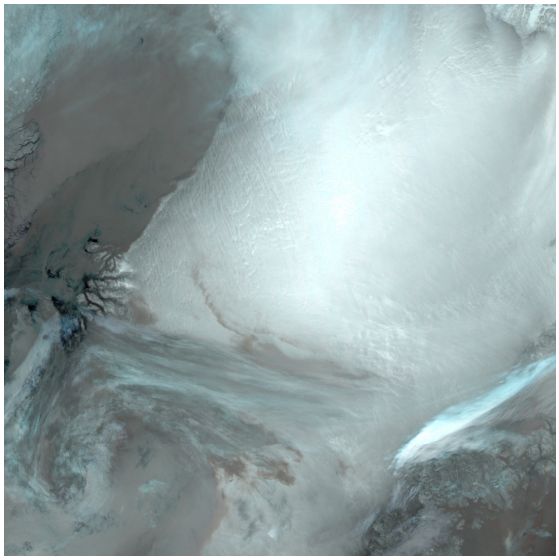

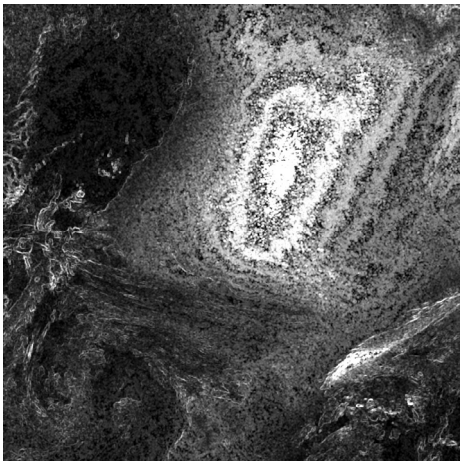

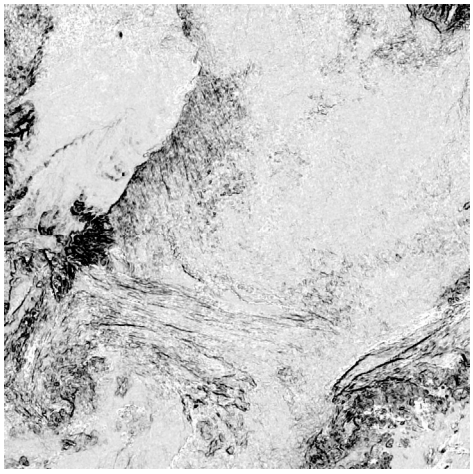

Figure 18. *An RGB scene from NOAA-18 of Greenland (tile ibla_79n45w in Figure 2) from 1st of January 2007 at 06:36 UTC (top), the corresponding* ***T37T12_text*** *feature (bottom left) and* ***T37T12_text*** *minus* ***T37_text*** *difference (bottom right). For the RGB scene, light areas are colder than dark areas, Cirrus is blue and Stratus and semi-transparent low clouds are brown coloured. For the bottom figures, dark areas have lower values than light areas.*

The typical conditions over Greenland are conditions of very cold temperatures. The large positive values shown in **T37T12_text** (bottom left) indicate considerable amounts of noise. In addition, the large scale circular patterns are related to the very low radiometric accuracy (especially for **T37**) for extremely low temperatures. Under these conditions a change of only one digital count can be related to temperature difference of several degrees Kelvin. The temperature in this area is around 220K. In this case **T37_text** (bottom right) appears no more sensitive to noise than **T37T12_text** although coastal areas and leads are clearly visible.

5.4 Detailed explanation of tests in the INS CM test sequence

Test 1 (**T11T37 > 0.5 K & T37T12_text < 0.6 K**) classifies most of the clouds, which are both warmer then the earth surface and somewhat transparent and/or are water clouds, cloud types abundantly present during Arctic winter. The included texture feature filters out most cloud free pixels which would be classified as clouds due to noise. In the NS CM v1.6 this test is used with a lower offset without any texture restraint, consequently causing large cloud free areas to be incorrectly classified as water clouds. Test 1 of the INS test sequence returns CM = 3 (cloud filled) if the pixel is deemed cloudy.

Test 2 (**T11TS < -18 K**) detects clouds which are significantly colder than the model skin surface temperature. The static offset used in this test is very large due to the model surface temperature at times overestimating the surface temperature in the order of 20 K. Even with the large static offset, misclassifications of some cloud free areas are inevitable. Despite this, this test is placed high in the test sequence order as it still is a relatively safe test. This test returns CM = 3 (cloud filled) if the pixel is classed here.

Test 3 (**T37T12 > 1.9 K & T37_text < 1.9 K**) detects semi-transparent Cirrus. This test also exists in the original NS CM sequence, with approximately similar threshold settings. The major difference here is that the **T37_text** feature is included to filter out the areas including leads and mixed water and ice. This test returns CM = 2 (cloud contaminated /filled with semi-transparent clouds) if the pixel is classed here.

Test 4 (**T37T12 < -1.6 K & T37T12_text < 0.6 K**) detects thin near-surface clouds, presumably water clouds, which are warmer than the earth surface. The persistent very stable conditions of the Arctic winter allow for many semi-transparent water clouds to be detected. The combined effect of **T37T12** < 0 for water clouds (due to low emissivity at T37) and **T37T12** < 0 for warm transparent clouds (due to high transmissivity) gives relatively large negative **T37T12** values for warm semi-transparent water clouds, which are common in the Arctic during winter.
This test is not redundant to test 1, because the threshold of the T37T12 feature is adapted here to detect thin clouds, while the T11T37 threshold in test 1 is optimised for rather thick water clouds. Consequently, this test returns CM = 2 (cloud contaminated /filled with transparent clouds) if the pixel is classed here.

Test 5 (**T11TS > 3 K & T11T37 > 0.3 K & T37T12 < -0.4 K & T37T12_text < 0.6 K**) is devised to detect warm opaque clouds like 'Black Stratus' which can either be water, ice or mixed phase in the Arctic. It is possible that the two tests, **T11T37 > 0.3 K & T37T12 < -0.4 K** are no longer necessary. They were originally included to avoid the detection of leads in the ice, which remains true, but the use of **T37_text** test is a more precise method of avoiding the detection of leads without filtering out real clouds. A comprehensive study across the entire Arctic showed this test to be less effective than anticipated due to the large model surface bias. The model surface temperature often too warm and as a consequence, less cloud is detected. Pixels captured by this test are classed CM = 3.

Test 6 (**T11T12 < -0.7 K**) is used to detect semi-transparent warm clouds and is a compliment to test 4. Normally, positive **T11T12** values indicate the presence of semi-transparent Cirrus and the **T11T12** test is used during daytime conditions for this purpose. Here the inverse of the **T11T12** Cirrus test is used to find semi-transparent warm clouds in strong inversions. The decreasing transmissivity with increasing wavelength results in smaller radiances at **T11**

compared to **T12.** This is due to that the radiance at **T11** containing, to larger extent, radiances from both the very cold surface and the cloud top temperatures. It's also debateable whether test 6 and test 4 should swap locations in the test sequence. The major advantage of test 6 is that it is not particularly sensitive to noise as test 4 may be. Note, preliminarily evaluation indicates that removing any one of the warm cloud tests decreases the detection of such clouds, and therefore both tests remained in the sequence.
Test 6 returns CM = 2 if the pixel is deemed cloudy here.

Test 7 (**T11T12 > 0.7 K & T37_text < 1.9 K**) is an extra ice cloud test and is complementary to test 3. This test is not sensitive to noise and with the inclusion of the **T37_text** feature, doesn't risk misclassifying leads in the ice. It is also debatable whether or not this test should be placed before test 3 in the test sequence. A preliminarily evaluation indicates that removing any one of the ice tests decreases the detection of Cirrus somewhat and therefore both tests have remained in the test sequence. Pixels captured by this test are classed CM = 2.

Test 8 (**T11T37 > 2 K**) is an extra water cloud and/ or semi-transparent warm clouds which have a clear such signal. This test was added late to the test sequence when it was apparent that some water clouds with a large **T11T37** signal were not classed in test 3 due to being filtered out for their large variance. With this relatively large offset more clouds can be detected without a substantial risk of misclassifying noise. Clouds detected here appear fairly opaque and are therefore classed as CM = 3.

6 Demonstration and validation of INS CM results

To run the test sequences on the aforementioned training targets is the only remotely quantitative validation method currently available for the INS CM.

The latest version of NS CM test sequence classes almost every training target as being transparently cloudy or cloud contaminated (see results in Section 4) and only slightly higher than 50 % of all situations are correctly classified. This can now be compared to the following corresponding results for the new INS CM test sequence, compared with the same training target dataset:

Cloud-free targets: 69 % correctly classified
Semi-transparent cloudy targets: 5 % correctly classified (24 % Opaque cloudy)
Opaque cloudy targets: 54 % correctly classified (11 % Semi-transparent cloudy)

An alternative presentation of results only concentrating on the performance of the binary value Cloud Mask (i.e., Cloudy or Cloud-free) yields:

Cloud-free: 69 % correct
Cloudy: 44 % correct

We notice that based on the target information we get a significant improvement in the treatment of the **Cloud-free** category where the number of misclassifications have decreased. Unfortunately, the skill for **Cloudy** targets has actually decreased at the same time which is a disappointment.

If looking at the corresponding results when running INS CM over land (land targets) the results are **68%** correctly classified cloud free**, 11%** correctly classified transparent cloudy and **58%** correctly classified opaque cloudy. Thus, the skill is much better for the cloudy targets. The reason for this is a bit difficult to understand but it could possibly be related to the fact that the labelling of targets was more confident due to the access of true observations at Barrow. Nevertheless, we note that the new test sequence performs decently good over land areas which has to be considered in the remaining development work when comparing results to the official land scheme of PPS (to be done in the near future).

Generally the results are quite ordinary for both the original NS CM and new INS CM test sequence and the inclusion of dynamical thresholds likely plays a large roll here. If the uncertainty involved in hand-picking and visually classifying the training targets is also taken into account, more doubts are shed on the validity of these results. It is often hard to visually decipher how opaque a near-opaque cloud should be before it is classed as a truly opaque cloud or how thin a very thin semi-transparent cloud should be before it is in fact classed as cloud free.

An alternative validation method is a qualitative evaluation where one determines the strengths and weaknesses of cloud masks by viewing entire scenes (visual inspection). Figures 19 a&b shows an example-scene from the Barrow test area. A large area of frontal clouds, large open areas of cloud free pack ice and some semi-transparent clouds over very cold surfaces are visible in the scene. For the associated cloud masks, grey colour represents semi-transparent or cloud contaminated pixels, white colour represents cloud filled pixels and black colour represents cloud free pixels or land. The area to the south of all of the following figures is northern Alaska. For the RGB image, cold temperatures can be seen by their bright colour whereas warmer temperatures are darker. For example; the ‘blue’ coloured clouds in the following scenes are cold semi-transparent Cirrus clouds whereas brown-reddish coloured clouds are water clouds or semi-transparent low clouds.

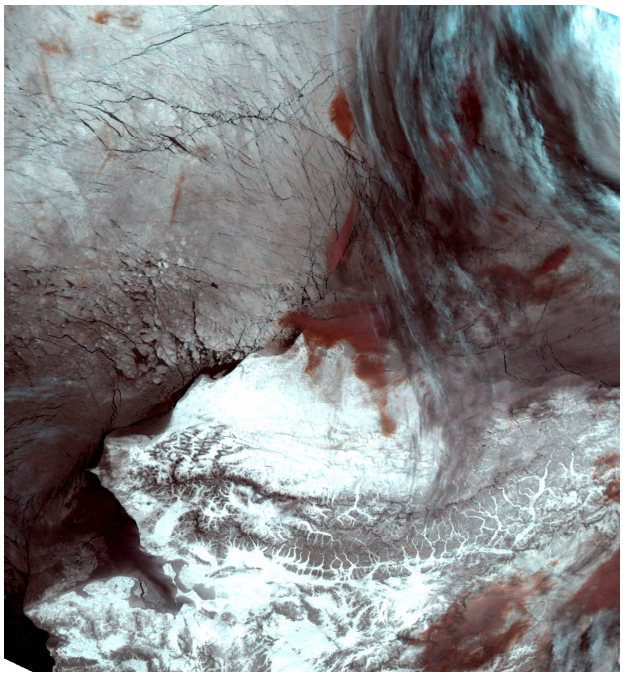

Figure 19a. *The Red, Green, Blue (RGB) image (**T37**, **T11**, **T12**) from NOAA-16 from December 19, 2001 at 16:39 UTC.*

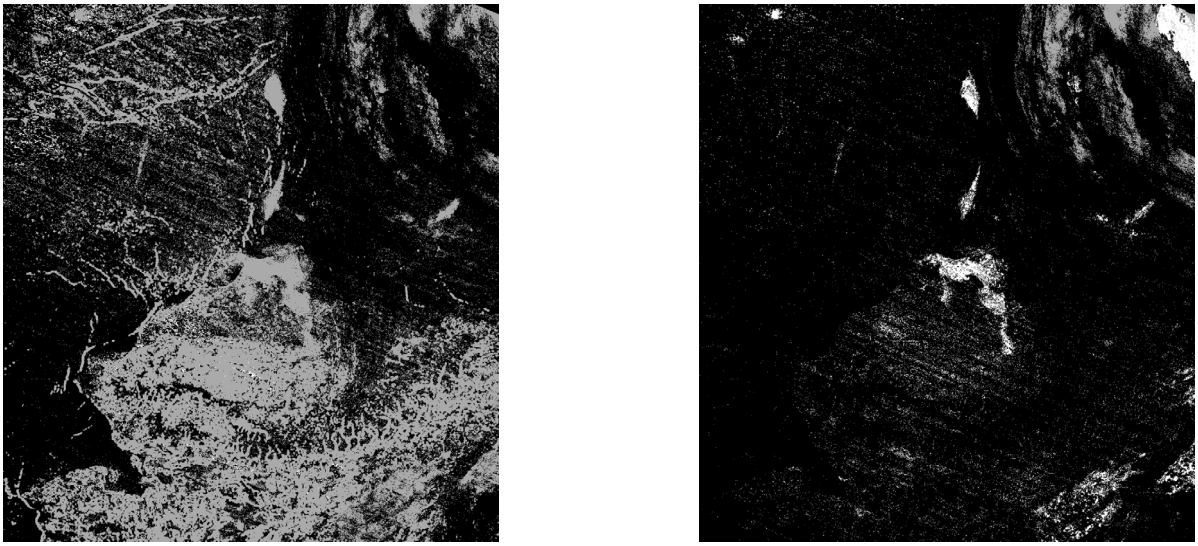

Figure 19b. *Results from the corresponding NS CM ~v1.4 (left) and INS CM (right) for NOAA-16 December 19, 2001 at 16:39 UTC. Since the Night Sea Cloud mask (left) is not intended for land areas the results over Northern Alaska should be ignored.*

Figure 19 indicates large differences between the cloud masks. The INS CM misses a great deal of the frontal cloud whereas the NS CM also misses most of them. Both the INS CM and NS CM capture the isolated pockets of semi-transparent cloud situated near the front and in the North West region of the scene, but the NS CM misclassifies many more cloud free pixels. The misclassified pixels are either due to leads or due to noise. The INS CM performance over land is passable (no notice should be taken to the performance of NS CM over land since the correct and official land PPS scheme has not been run here).

Figures 20 a & b show a scene from 5 January 2002 in which a cyclonic disturbance is clearly visible in the north of the scene. Warm semi-transparent clouds are clearly visible due south of the cyclonic system. These can be identified by the 'red-brownish' colour the clouds attain in the RGB due to the relatively large negative temperature difference between **T37** and the infrared channels. Large cloud free areas with distinct leads can be distinguished south of the band of warm semi-transparent clouds.

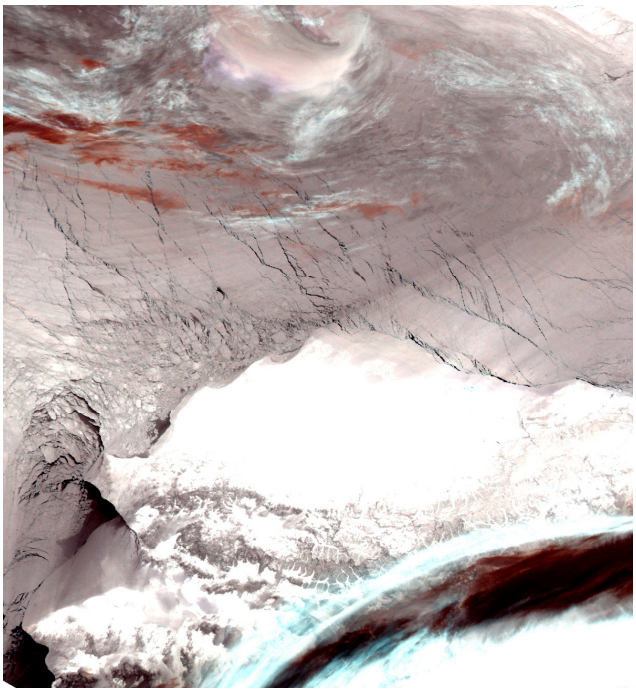

Figure 20a. *The RGB image from NOAA-16 of January 5, 2002 at 14:08 UTC.*

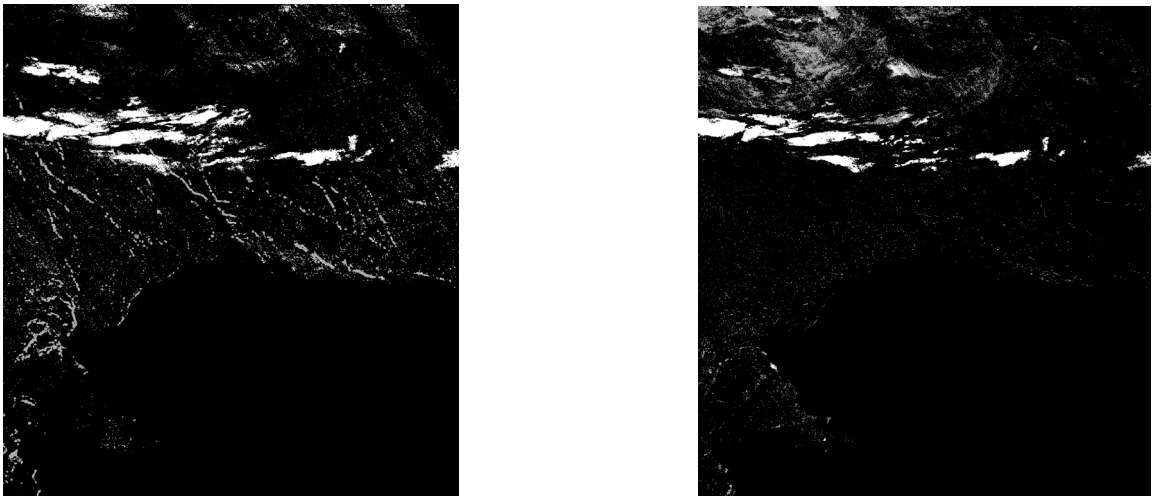

Figure 20b. *Results from the corresponding NS CM (left) and INS CM (right) for NOAA-16 January 5, 2002 at 14:08 UTC. Notice that results over land areas are masked out.*

The meteorological situation of 5 January 2002 is, as of yet largely overwhelming for the INS CM. Most of the clouds involved in this cyclonic disturbance appear multi-layered and have near-surface cloud top temperatures. The consequential lack of temperature contrast renders in the misclassification of clearly cloudy pixels as cloud free. Both test sequences easily

distinguish the warm semi-transparent clouds from the surface, but the NS CM once again misclassifies leads as cloudy.

Following are two scenes over the Barrow test area with large cloud free areas which have very cold model skin surface temperatures with some overlying semi-transparent clouds.

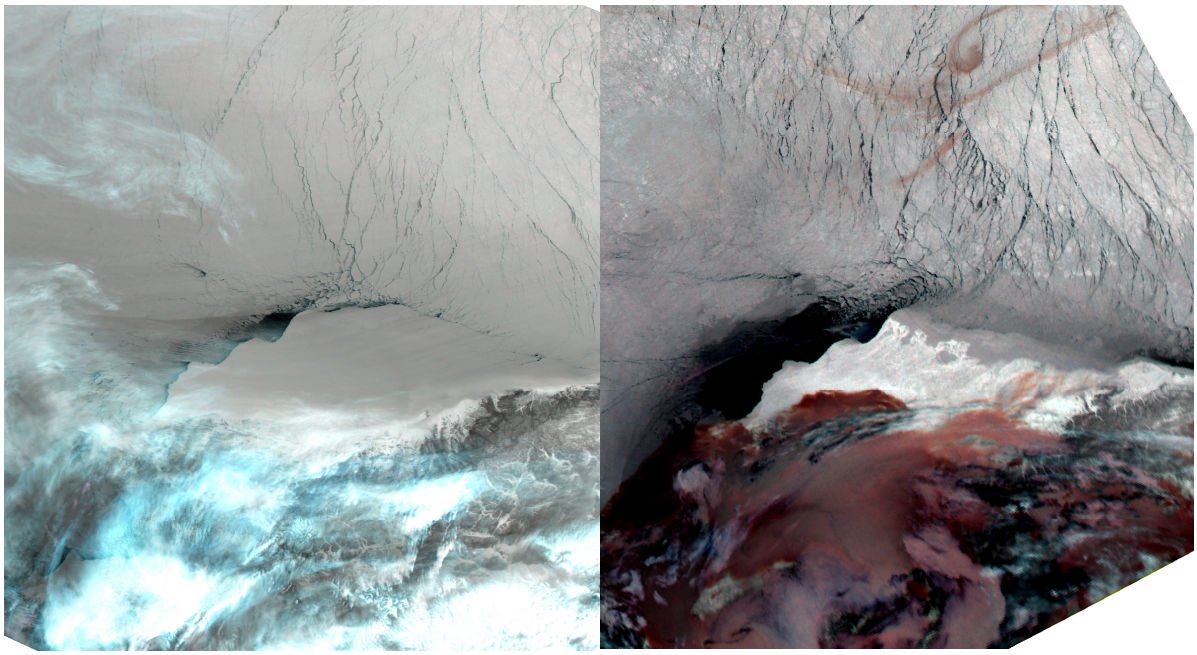

Figure 21a. *The RGB images for NOAA-16 February 4, 2002 at 13:47 UTC (left) and for NOAA-16 February 8, 2002 at 16:23 UTC (right).*

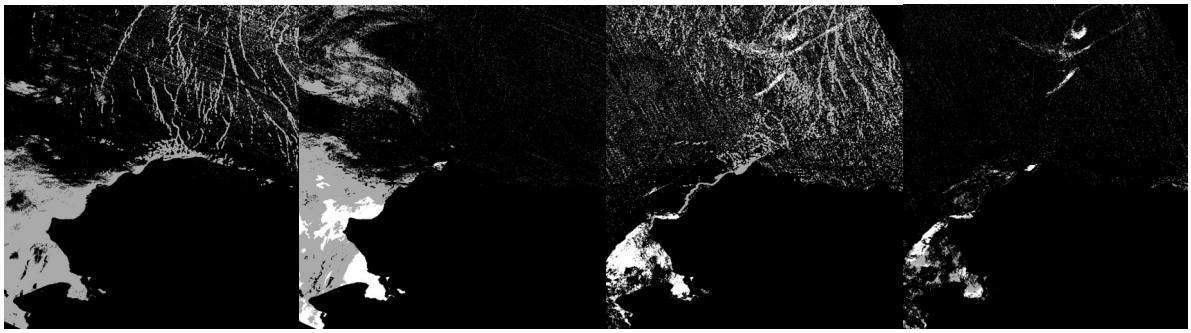

Figure 21b. *From left to right: 1) The NS CM of Feb 4, 2002 at 13:47 UTC. 2) The INS CM of Feb 4, 2002 at 13:47 UTC. 3) The NS CM of Feb 8, 2002 at 16:23 UTC. 4) The INS CM of Feb 8, 2002 at 16:23 UTC.*

These two scenes depict a climatologically common state of the Arctic winter, namely largely suppressed conditions with overlying semi-transparent clouds. Cold semi-transparent clouds can be found in the west of the February 4, 2002 scene and some warm semi-transparent clouds can be found in the east of the February 8, 2002 scene.

In both cases the INS CM correctly classifies more semi-transparent clouds than the NS CM and the NS CM misclassifies more cloud free areas, which are predictably predominately around leads than the INS CM does.

The Arctic winter also has some regular cyclonic windy conditions which diminish the strong inversion in the system somewhat. The makeup of the INS cloud mask is strongly influenced by the task of capturing clouds in very strong inversions, but as can be seen in Figure 22 a & b, the cloud mask has little problems in detecting clouds in and around this particular low pressure system.

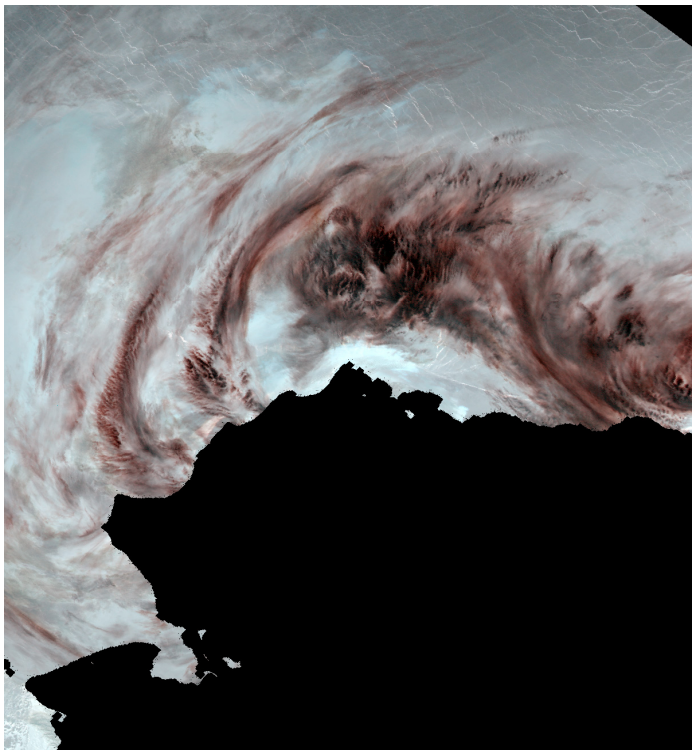

Figure 22a. *The RGB image from NOAA-16 over the Barrow test area of December 23, 2001 at 16:26 UTC.*

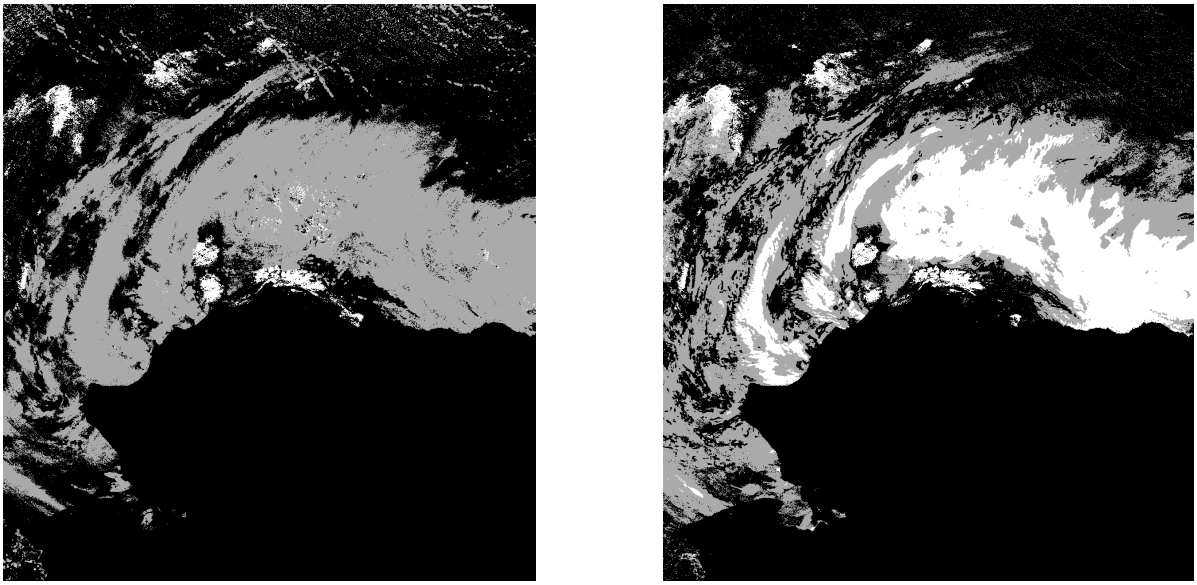

Figure 22b. *Results from the corresponding NS CM (left) and INS CM (right) for December 23, 2001 at 16:26 UTC.*

The INS CM captures most clouds but once again misses clouds with near surface temperature values seen in the western part of this scene. The current NS cloud mask is similarly successful for the large part but misses slighter more clouds around the fringe of the system and misclassifies some cloud free areas to the north of the scene.
As a final case, we demonstrate in Figure 23 the results of the quite complicated situation on the cover of this report. Again, it is evident that the INS CM method makes a significant improvement to the achieved cloud mask results even if we do not know the true cloudiness in this case.

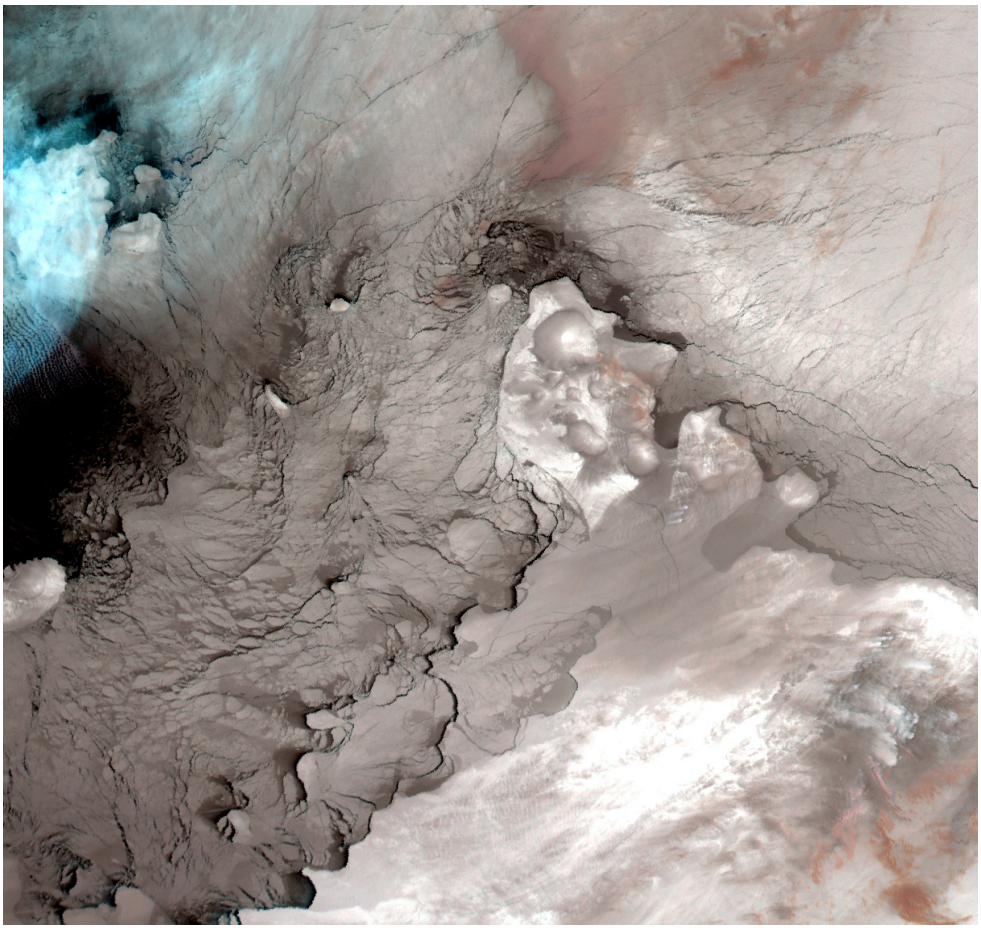

Figure 23a. *The RGB image from NOAA-18 over the Severnaya Zemlya area (tile ibla_79n90e in Figure 2) of January 31, 2007 at 03:09 UTC.*

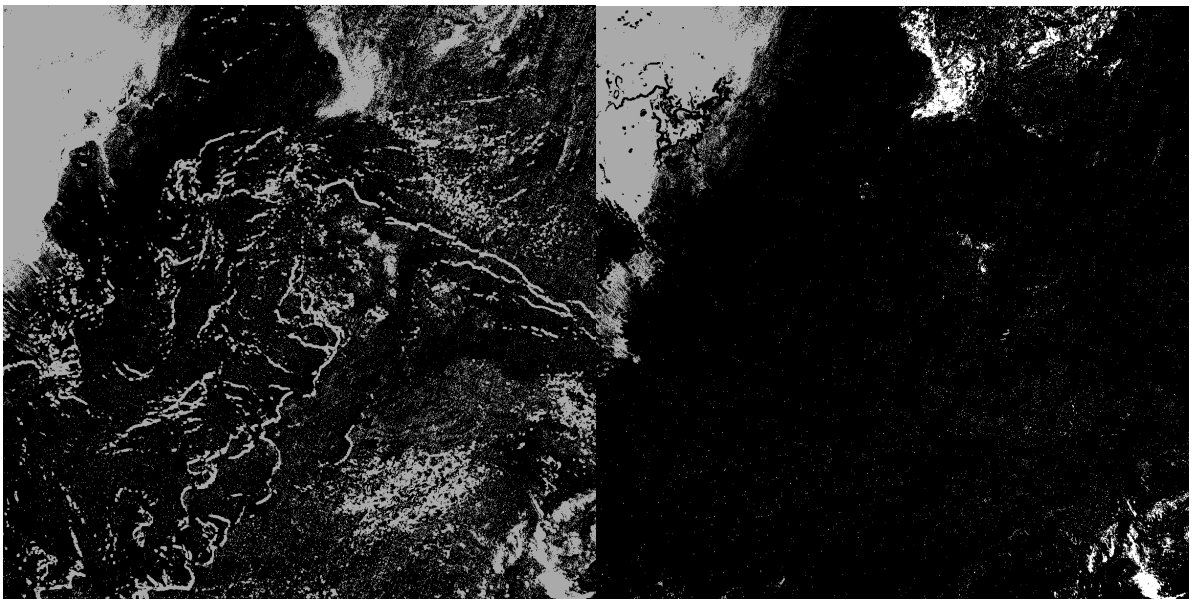

Figure 23b. *Results from the corresponding NS CM (left) and INS CM (right) for January 31, 2007 at 03:09 UTC.*

Finally, we can also present a first attempt of producing something similar to a monthly climatology based on the NS CM and INS CM test sequences in the Arctic region. Figure 24 shows the cloud frequency (in greyscale representation where bright values gives high cloud frequencies) in January 2007 computed from 62 NOAA AVHRR scenes (NOAA-17 and NOAA-18) over a region composed of tiles (from left to right) ibla_79n45w, ibla_79n00e and ibla_74n45e (see Figure 2). INS CM results (bottom panel) can be compared with the corresponding results of the default NS CM method (including "clear sky terminator" test, top panel) and the modified NS CM method (without "clear sky terminator" test, middle panel). We notice that the original NS CM method naturally gives almost completely overcast cloud conditions. Only for partly ice-free areas near and to the south of Svalbard we get lower frequencies than 100 %. More interesting is to compare the two lower panels. The difference is not very large but it is clear that results with INS CM give slightly lower values, most probably as an effect of the reduced misclassification of cloud-free areas over ice. We can also see that some features related to typical coastlines have disappeared or have been smoothed for INS CM. There are also some interesting differences in the monthly cloudiness features, especially in the partly ice-free parts of the studied region.

We cannot discuss these results more than qualitatively and further extensive validation and development work is required to get a better idea of the quality of INS CM results.

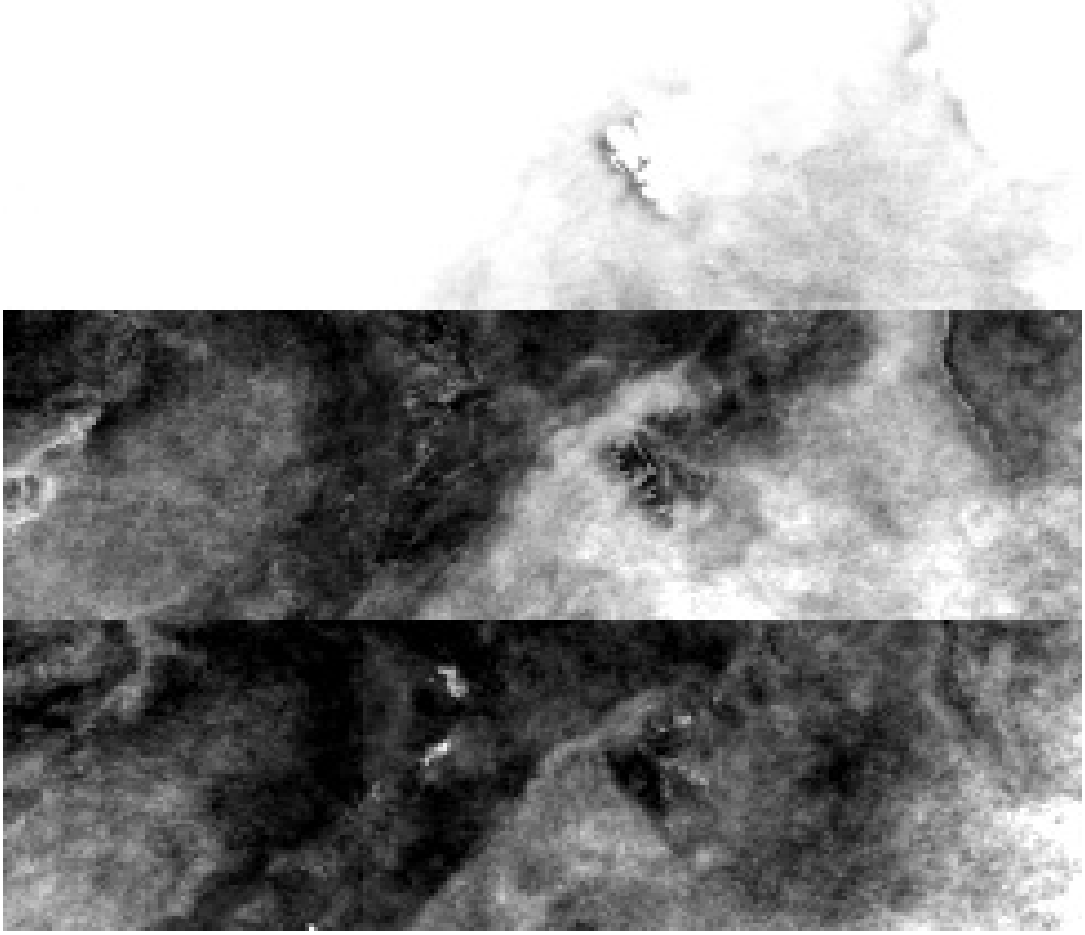

Figure 24. *Cloud frequencies (in %, displayed as a qualitative greyscale image where bright means high cloud frequency) in January 2007 computed from 62 NOAA AVHRR scenes (NOAA-17 and NOAA-18) over a region composed of tiles (from left to right) ibla_79n45w, ibla_79n00e and ibla_74n45e (see Figure 2). Frequencies in the interval between 50 -100 % are shown in white while a linear greyscale (i.e. black to white) is used in the range 15-50 %.*

7 Discussion and future plans

The new INS CM test sequence has showed improved results compared to NS CM but it also has some remaining limitations. The problem of detecting semi-transparent clouds with cloud top temperatures similar to the underlying surface temperature still remains. Also, multilayered clouds are practically indistinguishable when high clouds and their underlying clouds produces opposite signs of the same magnitude in temperature difference images based on two infrared channels. In addition, such clouds have often effective brightness temperatures rather close to the surface temperature which means that not even the cold cloud test (Test 2) will detect these clouds.

For the most part the inclusion of texture features in the sequence was a nice solution; however some clouds distinguishable by eye are not detected because they are filtered out by the makeshift cloud filter. Lifting the **T37T12_text** offset value may allow these clouds to be detected but at the cost of also misclassifying cloud free areas due to the noise in the area.

Importantly, the cloud masks dependency on model data makes the sequence quite vulnerable to errors. The model surface temperature is needed to compute the dynamical thresholds and the **T11TS** test is an important test in the detection of opaque cold clouds.

Another serious problem with the INS Cloud Mask or any cloud mask intended to be run in the harsh conditions like those found in the Arctic is the aforementioned problem of poor dynamical thresholds for very cold and very dry conditions. Currently dynamical thresholds are derived from a pre-computed look-up table which was generated from radiative transfer simulations based on the RTTOV radiative transfer model (Matricardi, 2001). However, because the common atmospheric state found during the Arctic winter is one of very low water vapour content at very low temperatures, problems arise. This atmospheric condition is sparsely represented amongst the cloud free atmospheric profiles used to generate the dynamical thresholds.

The tabulated values are extrapolated from the nearest atmospheric profiles and at such low surface temperatures and low water vapour content the derived dynamical threshold values do not appear physical. This is likely to be due to the extrapolated ‘distance’ to the nearest profile being too far. For example, the average dynamical threshold for the **T37T12** Cirrus test for the entire Arctic region during January 2007 is approximately 1.2K according to the corresponding lookup table. However, the expected dynamical threshold should rather be close to 0K for an Arctic atmosphere during the polar winter. Nevertheless, the dynamical thresholds act as a kind of noise filter for very cold temperatures so their use is not only causing problems for the cloud detection. As the surface temperature decreases the radiances diminish towards low radiance/noise ratios, as mentioned earlier this is probably due to the fact that at such low temperatures the AVHRR channel calibrations are not sufficiently accurate. The very cold temperatures also affect the dynamical thresholds and the dynamical thresholds actually increase (erroneously) in size hence, effectively filtering out some noise. Naturally this behaviour of the dynamical thresholds also filters out some cloudy pixels.

This filtering effect from the dynamical thresholds appears to act as a complement to the included **T37T12_text** feature. Therefore, removing the dynamical thresholds may have some unwanted effects. If or when the dynamical thresholds are removed (or replaced with more

correct values), the clouds gained in the very cold areas after adjusting the static offsets due to the removal the dynamical thresholds may have the side-effect of some clouds no longer being detected in the slighter warmer areas, a clear disadvantage of using purely static thresholds.

This report describes the status of the Ice Night Sea (INS) Cloud Mask test sequence as it were defined and finally tested in August 2007. There are some remaining unresolved issues which could lead to a better cloud mask. For example, a few tests with a calculation of the variance tests over larger windows (e.g., 7x7 pixels instead of 5x5 pixels) appeared to improve results further. However, current preliminary results with INS tests show an improvement from the previous NS cloud mask results. It is recommended that more time will have to be spent in resolving the remaining issues with the INS test sequence starting with improved dynamical thresholds. It is also recommended to assess whether or not to use the INS sequence over land as the harsh Arctic conditions over land (especially Greenland) are quite similar to conditions experienced over pack ice and some qualitative evaluation shows that cloud detection can also be improved over land using INS.

References

Dybbroe, A., Thoss, A. and Karlsson, K.-G., 2004a: NWCSAF AVHRR cloud detection and analysis using dynamic thresholds and radiative transfer modeling - Part I: Algorithm description, *J. Appl. Meteor,.* **44**, 39-54.

Dybbroe A., Thoss, A. and Karlsson, K.-G., 2004b: NWCSAF AVHRR cloud detection and analysis using dynamic thresholds and radiative transfer modeling - Part II: Validation, *J. Appl. Meteor.,* **44***,* 55-71.

Matricardi, M.F., F. Chevallier and S. Tjemkes, 2001: An improved general fast radiative transfer model for the assimilation of radiance observations, ECMWF Tech. Memo. 345, 44 pp.

Schulz, J., P. Albert, H.-D. Behr, S. Dewitte, B. Dürr, A.Gratzki, R. Hollmann, K.-G. Karlsson, T. Manninen, R. Müller, R. Roebeling, N. Selbach, A. Tetzlaff, W. Thomas, M. Werscheck,and Antoine Zelenka, 2005: Operational climate monitoring from space: the Satellite Application Facility on Climate Monitoring, *Proc. NOAA 29th Annual Climate Diagnostics and Prediction Workshop October 18-22, 2004, Madison, Wisconsin*.

Spangenberg et al. 2005: Retrieval of Cloud Phase Using the Moderate Resolution Imaging Spectroradiometer Data during the Mixed-Phase Arctic Cloud Experiment, 15th ARM Science Team Meeting Proceedings, Daytona Beach, Florida, March 14-18, 2004.

Sus, O., 2007: The effects of substituting the AVHRR 3.7 µm channel with the 1.6 µm channel on cloud masking in the Inner Arctic, Master Thesis (under review), Department of Geoscience - Physical Geography, University of Trier, Germany, 118 pp.

SMHIs publiceringar

SMHI ger ut sex rapportserier. Tre av dessa, R-serierna är avsedda för internationell publik och skrivs därför oftast på engelska. I de övriga serierna används det svenska språket.

Seriernas namn	**Publiceras sedan**
RMK (Rapport Meteorologi och Klimatologi)	1974
RH (Rapport Hydrologi)	1990
RO (Rapport Oceanografi)	1986
METEOROLOGI	1985
HYDROLOGI	1985
OCEANOGRAFI	1985

I serien METEOROLOGI har tidigare utgivits:

1985

1 Hagmarker, A. (1985)
Satellitmeteorologi.

2 Fredriksson, U., Persson, Ch., Laurin, S. (1985)
Helsingborgsluft.

3 Persson, Ch., Wern, L. (1985)
Spridnings- och depositionsberäkningar för av fallsförbränningsanläggningar i Sofielund och Högdalen.

4 Kindell, S. (1985)
Spridningsberäkningar för SUPRAs anläggningar i Köping.

5 Andersson, C., Kvick, T. (1985)
Vindmätningar på tre platser på Gotland. Utvärdering nr 1.

6 Kindell, S. (1985)
Spridningsberäkningar för Ericsson, Ingelstafabriken.

7 Fredriksson, U. (1985)
Spridningsberäkningar för olika plymlyft vid avfallsvärmeverket Sävenäs.

8 Fredriksson, U., Persson, Ch. (1985)
NO_x- och NO_2-beräkningar vid Vasaterminalen i Stockholm.

9 Wern, L. (1985)
Spridningsberäkningar för ASEA transformers i Ludvika.

10 Axelsson, G., Eklind, R. (1985)
Ovädret på Östersjön 23 juli 1985.

11 Laurin, S., Bringfelt, B. (1985)
Spridningsmodell för kväveoxider i gatumiljö.

12 Persson, Ch., Wern, L. (1985)
Spridnings- och depositionsberäkningar för avfallsförbränningsanläggning i Sofielund.

13 Persson, Ch., Wern, L. (1985)
Spridnings- och depositionsberäkningar för avfallsförbränningsanläggning i Högdalen.

14 Vedin, H., Andersson, C. (1985)
Extrema köldperioder i Stockholm.

15 Krieg, R., Omstedt, G. (1985)
Spridningsberäkningar för Volvos planerade bilfabrik i Uddevalla.

16 Kindell, S. Wern, L. (1985)
Luftvårdsstudie avseende industrikombinatet i Nynäshamn (koncentrations- och luktberäkningar).

17 Laurin, S., Persson, Ch. (1985)
Beräknad formaldehydspridning och deposition från SWEDSPANs spånskivefabrik.

18 Persson, Ch., Wern, L. (1985)
Luftvårdsstudie avseende industri-kombinatet i Nynäshamn – depositions-beräkningar av koldamm.

19 Fredriksson, U. (1985)
Luktberäkningar för Bofors Plast i Ljungby, II.

20 Wern, L., Omstedt, G. (1985)
Spridningsberäkningar för Volvos planerade bilfabrik i Uddevalla - energicentralen.

21 Krieg, R., Omstedt, G. (1985)
Spridningsberäkningar för Volvos planerade bilfabrik i Uddevalla - kompletterande beräkningar för fabrikerna.

22 Karlsson, K.-G. (1985)
Information från Meteosat - forskningsrön och operationell tillämpning.

23 Fredriksson, U. (1985)
Spridningsberäkningar för AB Åkerlund & Rausings fabrik i Lund.

24 Färnlöf, S. (1985)
Radarmeteorologi.

25 Ahlström, B., Salomonsson, G. (1985)
Resultat av 5-dygnsprognos till ledning för isbrytarverksamhet vintern 1984-85.

26 Wern, L. (1985)
Avesta stadsmodell.

27 Hultberg, H. (1985)
Statistisk prognos av yttemperatur.

1986

1 Krieg, R., Johansson, L., Andersson, C. (1986)
Vindmätningar i höga master, kvartalsrapport 3/1985.

2 Olsson, L.-E., Kindell, S. (1986)
Air pollution impact assessment for the SABAH timber, pulp and paper complex.

3 Ivarsson, K.-I. (1986)
Resultat av byggväderprognoser - säsongen 1984/85.

4 Persson, Ch., Robertson, L. (1986)
Spridnings- och depositionsberäkningar för en sopförbränningsanläggning i Skövde.

5 Laurin, S. (1986)
Bilavgaser vid intagsplan - Eskilstuna.

6 Robertson, L. (1986)
Koncentrations- och depositionsberäkningar för en sopförbränningsanläggning vid Ryaverken i Borås.

7 Laurin, S. (1986)
Luften i Avesta - föroreningsbidrag från trafiken.

8 Robertson, L., Ring, S. (1986)
Spridningsberäkningar för bromcyan.

9 Wern, L. (1986)
Extrema byvindar i Orrefors.

10 Robertson, L. (1986)
Koncentrations- och depositionsberäkningar för Halmstads avfallsförbränningsanläggning vid Kristinehed.

11 Törnevik, H., Ugnell (1986)
Belastningsprognoser.

12 Joelsson, R. (1986)
Något om användningen av numeriska prognoser på SMHI (i princip rapporten till ECMWF).

13 Krieg, R., Andersson, C. (1986)
Vindmätningar i höga master, kvartalsrapport 4/1985.

14 Dahlgren, L. (1986)
Solmätning vid SMHI.

15 Wern, L. (1986)
Spridningsberäkningar för ett kraftvärmeverk i Sundbyberg.

16 Kindell, S. (1986)
Spridningsberäkningar för Uddevallas fjärrvärmecentral i Hovhult.

17 Häggkvist, K., Persson, Ch., Robertson, L (1986)
Spridningsberäkningar rörande gasutsläpp från ett antal källor inom SSAB Luleåverken.

18 Krieg, R., Wern, L. (1986)
En klimatstudie för Arlanda stad.

19 Vedin, H. (1986)
Extrem arealnederbörd i Sverige.

20 Wern, L. (1986)
Spridningsberäkningar för lösningsmedel i Tibro.

21 Krieg, R., Andersson, C. (1986)
Vindmätningar i höga master - kvartalsrapport 1/1986.

22 Kvick, T. (1986)
Beräkning av vindenergitillgången på några platser i Halland och Bohuslän.

23 Krieg, R., Andersson, C. (1986)
Vindmätningar i höga master - kvartalsrapport 2/1986.

24 Persson, Ch. (SMHI), Rodhe, H. (MISU), De Geer, L.-E. (FOA) (1986)
Tjernobylolyckan - En meteorologisk analys av hur radioaktivitet spreds till Sverige.

25 Fredriksson, U. (1986)
Spridningsberäkningar för Spendrups bryggeri, Grängesberg.

26 Krieg, R. (1986)
Beräkningar av vindenergitillgången på några platser i Skåne.

27 Wern, L., Ring, S. (1986)
Spridningsberäkningar, SSAB.

28 Wern, L., Ring, S. (1986)
Spridningsberäkningar för ny ugn, SSAB II.

29 Wern, L. (1986)
Spridningsberäkningar för Volvo Hallsbergverken.

30 Fredriksson, U. (1986)
SO_2-halter från Hammarbyverket kring ny arena vid Johanneshov.

31 Persson, Ch., Robertson, L., Häggkvist, K. (1986)
Spridningsberäkningar, SSAB - Luleåverken.

32 Kindell, S., Ring, S. (1986)
Spridningsberäkningar för SAABs planerade bilfabrik i Malmö.

33 Wern, L. (1986)
Spridningsberäkningar för svavelsyrafabrik i Falun.

34 Wern, L., Ring, S. (1986)
Spridningsberäkningar för Västhamnsverket HKV1 i Helsingborg.

35 Persson, Ch., Wern, L. (1986)
Beräkningar av svaveldepositionen i Stockholmsområdet.

36 Joelsson, R. (1986)
USAs månadsprognoser.

37 Vakant nr.

38 Krieg, R., Andersson, C. (1986)
Utemiljön vid Kvarnberget, Lysekil.

39 Häggkvist, K. (1986)
Spridningsberäkningar av freon 22 från Ropstens värmepumpverk.

40 Fredriksson, U. (1986)
Vindklassificering av en plats på Hemsön.

41 Nilsson, S. (1986)
Utvärdering av sommarens (1986) använda konvektionsprognoshjälpmedel.

42 Krieg, R., Kvick, T. (1986)
Vindmätningar i höga master.

43 Krieg, R., Fredriksson, U. (1986)
Vindarna över Sverige.

44 Robertson, L. (1986)
Spridningsberäkningar rörande gasutsläpp vid ScanDust i Landskrona - bestämning av cyanvätehalter.

45 Kvick, T., Krieg, R., Robertson, L. (1986)
Vindförhållandena i Sveriges kust- och havsband, rapport nr 2.

46 Fredriksson, U. (1986)
Spridningsberäkningar för en planerad panncentral vid Lindsdal utanför Kalmar.

47 Fredriksson, U. (1986)
Spridningsberäkningar för Volvo BMs fabrik i Landskrona.

48 Fredriksson, U. (1986)
Spridningsberäkningar för ELMO-CALFs fabrik i Svenljunga.

49 Häggkvist, K. (1986)
Spridningsberäkningar rörande gasutsläpp från syrgas- och bensenupplag inom SSAB Luleåverken.

50 Wern, L., Fredriksson, U., Ring, S. (1986)
Spridningsberäkningar för lösningsmedel i Tidaholm.

51 Wern, L. (1986)
Spridningsberäkningar för Volvo BM ABs anläggning i Braås.

52 Ericson, K. (1986)
Meteorological measurements performed May 15, 1984, to June, 1984, by the SMHI.

53 Wern, L., Fredriksson, U. (1986)
Spridningsberäkning för Kockums Plåtteknik, Ronneby.

54 Eriksson, B. (1986)
Frekvensanalys av timvisa temperaturobservationer.

55 Wern, L., Kindell, S. (1986)
Luktberäkningar för AB ELMO i Flen.

56 Robertson, L. (1986)
Spridningsberäkningar rörande utsläpp av NO_x inom Fagersta kommun.

57 Kindell, S. (1987)
Luften i Nässjö.

58 Persson, Ch., Robertson, L. (1987)
Spridningsberäkningar rörande gasutsläpp vid ScanDust i Landskrona - bestämning av cyanväte.

59 Bringfelt, B. (1987)
Receptorbaserad partikelmodell för gatumiljömodell för en gata i Nyköping.

60 Robertson, L. (1987)
Spridningsberäkningar för Varbergs kommun. Bestämning av halter av SO_2, CO, NO_x samt några kolväten.

61 Vedin, H., Andersson, C. (1987)
E 66 - Linderödsåsen - klimatförhållanden.

62 Wern, L., Fredriksson, U. (1987)
Spridningsberäkningar för Kockums Plåtteknik, Ronneby. 2.

63 Taesler, R., Andersson, C., Wallentin, C., Krieg, R. (1987)
Klimatkorrigering för energiförbrukningen i ett eluppvärmt villaområde.

64 Fredriksson, U. (1987)
Spridningsberäkningar för AB Åetå-Trycks planerade anläggning vid Kungens Kurva.

65 Melgarejo, J. (1987)
Mesoskalig modellering vid SMHI.

66 Häggkvist, K. (1987)
Vindlaster på kordahus vid Alviks Strand - numeriska beräkningar.

67 Persson, Ch. (1987)
Beräkning av lukt och föroreningshalter i luft runt Neste Polyester i Nol.

68 Fredriksson, U., Krieg, R. (1987)
En överskalig klimatstudie för Tornby, Linköping.

69 Häggkvist, K. (1987)
En numerisk modell för beräkning av vertikal momentumtransport i områden med stora råhetselement. Tillämpning på ett energiskogsområde.

70 Lindström, Kjell (1987)
Weather and flying briefing aspects.

71 Häggkvist, K. (1987)
En numerisk modell för beräkning av vertikal momentumtransport i områden med stora råhetselement. En koefficientbestämning.

72 Liljas, E. (1988)
Förbättrad väderinformation i jordbruket - behov och möjligheter (PROFARM).

73 Andersson, Tage (1988)
Isbildning på flygplan.

74 Andersson, Tage (1988)
Aeronautic wind shear and turbulence.
A review for forecasts.

75 Källberg, P. (1988)
Parameterisering av diabatiska processer i numeriska prognosmodeller.

76 Vedin, H., Eriksson, B. (1988)
Extrem arealnederbörd i Sverige 1881 - 1988.

77 Eriksson, B., Carlsson, B., Dahlström, B. (1989)
Preliminär handledning för korrektion av nederbördsmängder.

78 Liljas, E. (1989)
Torv-väder. Behovsanalys med avseende på väderprognoser och produktion av bränsletorv.

79 Hagmarker, A. (1991)
Satellitmeteorologi.

80 Lövblad, G., Persson, Ch. (1991)
Background report on air pollution situation in the Baltic states - a prefeasibility study.
IVL Publikation B 1038.

81 Alexandersson, H., Karlström, C., Larsson-McCann, S. (1991)
Temperaturen och nederbörden i Sverige 1961-90. Referensnormaler.

82 Vedin, H., Alexandersson, H., Persson, M. (1991)
Utnyttjande av persistens i temperatur och nederbörd för vårflödesprognoser.

83 Moberg, A. (1992)
Lufttemperaturen i Stockholm 1756 - 1990. Historik, inhomogeniteter och urbaniseringseffekt.
Naturgeografiska Institutionen, Stockholms Universitet.

84 Josefsson, W. (1993)
Normalvärden för perioden 1961-90 av globalstrålning och solskenstid i Sverige.

85 Laurin, S., Alexandersson, H. (1994)
Några huvuddrag i det svenska temperatur-klimatet 1961 - 1990.

86 Fredriksson, U. och Ståhl, S. (1994)
En jämförelse mellan automatiska och manuella fältmätningar av temperatur och nederbörd.

87 Alexandersson, H., Eggertsson Karlström, C. och Laurin S. (1997).
Några huvuddrag i det svenska nederbördsklimatet 1961-1990.

88 Mattsson, J., Rummukainen, M. (1998)
Växthuseffekten och klimatet i Norden - en översikt.

89 Kindbom, K., Sjöberg, K., Munthe, J., Peterson, K. (IVL)
Persson, C. Roos, E., Bergström, R. (SMHI). (1998)
Nationell miljöövervakning av luft- och nederbördskemi 1996.

90 Foltescu, V.L., Häggmark, L (1998)
Jämförelse mellan observationer och fält med griddad klimatologisk information.

91 Hultgren, P., Dybbroe, A., Karlsson, K.-G. (1999)
SCANDIA – its accuracy in classifying LOW CLOUDS

92 Hyvarinen, O., Karlsson, K.-G., Dybbroe, A. (1999)
Investigations of NOAA AVHRR/3 1.6 μm imagery for snow, cloud and sunglint discrimination (Nowcasting SAF)

93 Bennartz, R., Thoss, A., Dybbroe, A. and Michelson, D. B. (1999)
Precipitation Analysis from AMSU (Nowcasting SAF)

94 Appelqvist, Peter och Anders Karlsson (1999)
Nationell emissionsdatabas för utsläpp till luft - Förstudie.

95 Persson, Ch., Robertson L. (SMHI)
Thaning, L (LFOA). (2000)
Model for Simulation of Air and Ground Contamination Associated with Nuclear Weapons. An Emergency Preparedness Model.

96 Kindbom K., Svensson A., Sjöberg K., (IVL) Persson C., (SMHI) (2001)
Nationell miljöövervakning av luft- och nederbördskemi 1997, 1998 och 1999.

97 Diamandi, A., Dybbroe, A. (2001)
Nowcasting SAF
Validation of AVHRR cloud products.

98 Foltescu V. L., Persson Ch. (2001)
Beräkningar av moln- och dimdeposition i Sverigemodellen - Resultat för 1997 och 1998.

99 Alexandersson, H. och Eggertsson Karlström, C (2001)
Temperaturen och nederbörden i Sverige 1961-1990. Referensnormaler - utgåva 2.

100 Korpela, A., Dybbroe, A., Thoss, A. (2001)
Nowcasting SAF - Retrieving Cloud Top Temperature and Height in Semi-transparent and Fractional Cloudiness using AVHRR.

101 Josefsson, W. (1989)
Computed global radiation using interpolated, gridded cloudiness from the MESA-BETA analysis compared to measured global radiation.

102 Foltescu, V., Gidhagen, L., Omstedt, G. (2001)
Nomogram för uppskattning av halter av PM_{10} och NO_2

103 Omstedt, G., Gidhagen, L., Langner, J. (2002)
Spridning av förbränningsemissioner från småskalig biobränsleeldning
– analys av PM2.5 data från Lycksele med hjälp av två Gaussiska spridningsmodeller.

104 Alexandersson, H. (2002)
Temperatur och nederbörd i Sverige 1860 - 2001

105 Persson, Ch. (2002)
Kvaliteten hos nederbördskemiska mätdata

som utnyttjas för dataassimilation i MATCH-Sverige modellen".

106 Mattsson, J., Karlsson, K-G. (2002)
CM-SAF cloud products feasibility study in the inner Arctic region
Part I: Cloud mask studies during the 2001 Oden Arctic expedition

107 Kärner, O., Karlsson, K-G. (2003)
Climate Monitoring SAF - Cloud products feasibility study in the inner Arctic region.
Part II: Evaluation of the variability in radiation and cloud data

108 Persson, Ch., Magnusson, M. (2003)
Kvaliteten i uppmätta nederbördsmängder inom svenska nederbörskemiska stationsnät

109 Omstedt, G., Persson Ch., Skagerström, M (2003)
Vedeldning i småhusområden

110 Alexandersson, H., Vedin, H. (2003)
Dimensionerande regn för mycket små avrinningsområden

111 Alexandersson, H. (2003)
Korrektion av nederbörd enligt enkel klimatologisk metodik

112 Joro, S., Dybbroe, A.(2004)
Nowcasting SAF – IOP
Validating the AVHRR Cloud Top Temperature and Height product using weather radar data
Visiting Scientist report

113 Persson, Ch., Ressner, E., Klein, T. (2004)
Nationell miljöövervakning – MATCH-Sverige modellen
Metod- och resultatsammanställning för åren 1999-2002 samt diskussion av osäkerheter, trender och miljömål

114 Josefsson, W. (2004)
UV-radiation measured in Norrköping 1983-2003.

115 Martin, Judit, (2004)
Var tredje timme – Livet som väderobservatör

116 Gidhagen, L., Johansson, C., Törnquist, L. (2004)
NORDIC – A database for evaluation of dispersion models on the local, urban and regional scale

117 Langner, J., Bergström, R., Klein, T., Skagerström, M. (2004)
Nuläge och scenarier för inverkan på marknära ozon av emissioner från Västra Götalands län – Beräkningar för 1999

118 Trolez, M., Tetzlaff, A., Karlsson, K-G. (2005)
CM-SAF Validating the Cloud Top Height product using LIDAR data

119 Rummukainen, M. (2005)
Växthuseffekten

120 Omstedt, G. (2006)
Utvärdering av PM_{10} - mätningar i några olika nordiska trafikmiljöer

121 Alexandersson, H. (2006)
Vindstatistik för Sverige 1961-2004

122 Samuelsson, P., Gollvik, S., Ullerstig, A., (2006)
The land-surface scheme of the Rossby Centre regional atmospheric climate model (RCA3)

123 Omstedt, G. (2007)
VEDAIR – ett internetverktyg för beräkning av luftkvalitet vid småskalig biobränsleeldning
Modellbeskrivning och slutrapport mars 2007

124 Persson, G., Strandberg, G., Bärring, L., Kjellström, E. (2007)
Beräknade temperaturförhållanden för tre platser i Sverige – perioderna 1961-1990 och 2011-2040

125 Engart, M., Foltescu, V. (2007)
Luftföroreningar i Europa under framtida klimat

126 Jansson, A., Josefsson, W. (2007)
Modelling of surface global radiation and CIE-weighted UV-radiation for the period 1980-2000

127 Johnston, S., Karlsson, K-G. (2007)
METEOSAT 8 SEVIRI and NOAA Cloud Products. A Climate Monitoring SAF Comparison Study

Sveriges meteorologiska och hydrologiska institut
601 76 Norrköping · Tel 011-495 8000 · Fax 011-495 8001
www.smhi.se

ISSN 0283-7730